International Atomic Energy Agency

INDC(CCP)-296/L

INDC INTERNATIONAL NUCLEAR DATA COMMITTEE

EVALUATED NEUTRON DATA FOR PLUTONIUM-238
(Report No. 3)

A.B. Klepatskij, V.M. Maslov, Yu.V. Porodzinskij and
E.Sh. Sukhovitskij
Institute of Nuclear Power
Academy of Sciences of the Byelorussian SSR
Minsk, USSR

Translated by the IAEA

January 1989

IAEA NUCLEAR DATA SECTION, WAGRAMERSTRASSE 5, A-1400 VIENNA

INDC(CCP)-296/L

EVALUATED NEUTRON DATA FOR PLUTONIUM-238
(Report No. 3)

A.B. Klepatskij, V.M. Maslov, Yu.V. Porodzinskij and
E.Sh. Sukhovitskij
Institute of Nuclear Power
Academy of Sciences of the Byelorussian SSR
Minsk, USSR

Translated by the IAEA

January 1989

Reproduced by the IAEA in Austria
January 1989

89-00156

EVALUATED NEUTRON DATA FOR PLUTONIUM-238
(Report No. 3)

A.B. Klepatskij, V.M. Maslov, Yu.V. Porodzinskij and
E.Sh. Sukhovitskij
Institute of Nuclear Power
Academy of Sciences of the Byelorussian SSR
Minsk, USSR

ABSTRACT

The authors give the evaluation results for the characteristics of neutron interaction with the ^{238}Pu nucleus in the 10^{-5}-20 MeV region. Experimental data, as available at the end of 1986, were used for the evaluation. In spite of insufficient experimental information, it was possible to make a reliable evaluation by resorting extensively to contemporary theoretical models and the systematics of their parameters.

INTRODUCTION

The ^{238}Pu nucleus is a strong alpha emitter with a half-life of 87.75 years and, consequently, an intensive heat source. Therefore, ^{238}Pu is used in thermoelectric generators to produce electric power in space vehicles and also in pace makers. Its spontaneous fission half-life is $(5.0 \pm 0.6) \times 10^{10}$ years ($\bar{\nu}_{sf} = 2.28 \pm 0.08$).

Plutonium-238 can be obtained by irradiation in the neutron flux of a reactor. Its concentration during reactor operation attains saturation at a fairly low level. In thermal reactors the fraction of ^{238}Pu in the total mass of plutonium is ~ 1-1.5% [1], while in plutonium-fuelled fast reactors it drops to 0.5% since the production/disappearance ratio of ^{238}Pu is lower in the fast reactor than in the thermal reactor [2]. The use of regenerated uranium fuel increases the fraction of ^{238}Pu in the total mass to ~ 4.8% [2].

The accuracies required for calculation of the reactivity effects and other characteristics of fast reactors in the case of ^{238}Pu are: ~ 15%

for $(\bar{\nu}\sigma_{nf}-\sigma_a)$, ~ 7% for σ_{nf}, ~ 4% for $\bar{\nu}_p$, ~ 20% for $\sigma_{n\gamma}$ (for thermal reactors 10% for $\sigma_{n\gamma}$) [1]. The (n,3n) reaction cross-section for ^{238}Pu, which leads to the formation of ^{236}Pu, needs to be known with ~ 40% accuracy. The above accuracies for neutron cross-sections are sufficient also for the calculation of the fraction of ^{238}Pu in the total mass of fuel.

In the present study we describe the results of evaluation of all types of ^{238}Pu neutron cross-sections in the 10^{-5}-20 MeV region. For ^{238}Pu, experimental information is limited. In the fast neutron energy region, only the fission cross-section has been measured. Therefore, theoretical models were used to a great extent in order to evaluate and predict the neutron cross-sections. Table 1 gives the energies Q and thresholds T of the various reactions of neutrons with the ^{238}Pu nucleus. The value of the threshold (for negative Q) was obtained from the expression:

$$T = \frac{M + M_{238}}{M_{238}}(-Q) = \frac{1,0086652 + 238,049582}{238,049582}(-Q) =$$
$$= 1,004237(-Q),$$

where M_n is the neutron mass and M_{238} the mass of the ^{238}Pu nucleus.

In the energy region considered the cross-sections for reactions with charged-particle emission are negligibly small, owing to the Coulomb barrier, and were not taken into account in the present study.

The level scheme of the ^{238}Pu nucleus taken in the evaluation is given in Table 2 [5].

1. NUCLEAR DATA FOR ^{238}Pu IN THE RESOLVED RESONANCE REGION FROM 10^{-5} TO 500 eV

So far the region of resolved resonances of ^{238}Pu have not been studied satisfactorily - the resonances have been identified reliably only up to ~ 500 eV with an average distance of ~ 10 eV between resonances. The peculiarity of this isotope lies in the presence of anomalously large

resonances in the fission cross-section, which may be attributed to the double-humped structure of the fission barrier.

1.1. Experimental data for ^{238}Pu in the resolved resonance region

In the resolved resonance region of ^{238}Pu the following experimental data are known:

1. Young and co-workers [6] measured the total cross-section σ_t in the 0.008-6500 eV region. The resonance paramaters were obtained up to 200 eV. Owing to insufficient resolution the resonances with an energy above 18.562 eV were analysed by the area method, for which they took $\Gamma_\gamma + \Gamma_f = 38$ meV. The cross-sections in the region up to the first resonance were described for $\sigma_p = 17 \times 10^{-28}$ m^2.
2. Gerasimov [7] measured fission cross-section σ_{nf} in the 2.4×10^{-2}-420 eV energy interval with a very low resolution and determined the fission areas under five resonances.
3. Stubbins and co-workers [8] measured the ^{238}Pu fission cross-section and obtained the fission areas under 16 resonances up to 280 eV.
4. Silbert and co-workers [9, 10] measured the fission and capture cross-sections and areas under the ^{238}Pu resonances in the 18-500 eV region. From the analysis of these data the authors obtained the neutron and fission widths, assuming a constant radiative capture width of $\bar{\Gamma}_\gamma = 34$ meV.
5. Budtz-Jorgensen and co-workers [11] measured σ_{nf} in the 5 eV-10 MeV region and obtained the fission areas under the resonances up to 500 eV. The energy resolution in the resonance energy region is about twice as high as in Refs [9, 10]. The authors detected a resonance at 312.4 eV, which had not been described in other studies. The fission and radiative capture areas from Refs [7-11] are shown in Table 1.1. For each

resonance, starting from the fourth, the last line gives the evaluated values of the areas. For resonances where there is one measurement, the latter is taken as evaluated.

Apart from the series of data described above, there are measurements of the ^{238}Pu neutron cross-sections at thermal energy (Table 1.2).

1.2. Evaluated resonance parameters of ^{238}Pu

At the first stage of evaluation we determined the widths of the first three resonances (2.885, 9.975 and 18.562 eV), which had been subjected to shape analysis in Ref. [6], and obtained the total and neutron widths for them. Combining these data with the results of Ref. [8] we obtained for them the fission widths and, consequently, radiative capture widths. The average radiation width for these three resonances was 34.8 meV, which agrees satisfactorily with $\langle\Gamma_\gamma\rangle$ = 34 meV taken in Ref. [10] at Young's recommendation after his re-evalaution of the data [6]. In the present study, a width of $\langle\Gamma_\gamma\rangle$ = (34 $\pm$ 6.1) meV was taken for the remaining resonances. The value of the error 6.1 meV is obtained from the assumption that $\langle\Gamma_\gamma\rangle$ is known with an accuracy of $\pm$ 10% and that the dispersion of the average value is $\pm$ 15%.

The fission and radiative capture areas under the resonances, together with the radiation width, fully determine the neutron and fission widths of the resonances. The radiative capture areas were taken from Ref. [10], and the fission areas were evaluated on the basis of available experimental data and are given in Table 1.1. The errors of the resonance parameters were calculated in the standard manner. The resonance at 285.7 eV is wide and lends itself well to shape analysis. Its neutron and fission widths were therefore obtained by averaging these values from Refs [10, 11]. For the 312.4 eV resonance the fission area is taken as 46 x 10^{-28} m^2, which reflects the ratio between the evaluated and measured [11] fission areas for the next resonance. Since for the 312.4 eV resonance there are no data on the radiative capture area, the Γ_n and Γ_f values for it were calculated on

the assumption of a ratio $\Gamma_\gamma/\Gamma_f \simeq 0.35$ obtained from the analysis of the values of σ_{nf} and $\sigma_{n\gamma}$ [10].

The last two resonances (510 and 518 eV) are fictitious and were used in order to compensate for the contribution of distant resonances.

It was decided to compensate for the contribution of the resonances lying below the binding energy by two negative resonances, whose parameters were chosen in the following manner. The capture width of both resonances was taken as $\langle\Gamma_\gamma\rangle$ = 34 meV. The energy of the first negative resonance (-10 eV) was taken rather arbitrarily at a distance of ~ <D>. The fission width of this resonance was taken as the average over the nearest positive resonances, 4.5 meV, and the neutron width was so chosen as to compensate for the negative value of interference scattering of the positive resonances. The energy of the second negative resonance (-0.4 eV) was obtained from the description of the energy dependence of σ_t and σ_{nf} in the region up to the first resonance, while the values of Γ_n and Γ_f were so chosen as to describe the cross-sections for E = 0.0253 eV. The potential scattering cross-section was taken as 11×10^{-28} m^2, which follows from the systematics for nuclei with a relative atomic mass of ~ 240 and from calculations by the optical model. Young and co-workers [6] described the total cross-section data using $\sigma_p = 17 \times 10^{-28}$ m^2, which cannot be regarded as satisfactory. Although they could not attribute the difference of 6×10^{-28} m^2 to the presence of the contribution of scattering on small-diameter PuO_2 particles and on water, we consider that these data nevertheless contain a neglected systematic error. For example, a 1% systematic error in the normalization of the value of transmission will result in an error of ~ 6×10^{-28} m^2 in the measured total cross-section.

The evaluated values of the resonance parameters of ^{238}Pu are given in Table 1.3. For all resonances, starting from the fourth, the average radiative capture width is taken.

The resonance parameters given here can be used to determine the cross-sections in the incident-neutron energy region up to 500 eV by the single-level Breit-Wigner formula. The evaluated neutron cross-sections at the thermal point calculated from these resonance parameters are compared in Table 1.4 with the evaluations of Derrien [17] and ENDF/B-V [18]. It will be seen that all three evaluations agree within experimental errors although the ENDF/B-V data [18] are somewhat higher for σ_t and $\sigma_{n\gamma}$.

In Fig. 1.1 the evaluated cross-sections are compared with the experimental data for σ_t [6] and σ_{nf} [7] in the thermal region. It will be seen that the evaluted σ_t is ~ 6 x 10^{-28} m^2 lower than the data of Ref. [6] - this corresponds to the difference in the potential scattering cross-section values taken. This difference is maintained in the "dips" of the total cross-section curve in the entire resonance region.

1.3. Average resonance parameters from the resolved resonance region

We used the method described in Ref. [19] to determine the average parameters of the s-wave neutron resonances, taking into account the possible presence of a small p-resonance contribution. Calculations showed that in the region up to 500 eV about 7% resonances were missing. Making allowances for this, we obtained the following average values: $\langle D \rangle_{ev.}$ = (9.103 ± 0.6) eV, $\langle \Gamma_n^o \rangle_{ev.}$ = (1.126 ± 0.22) $meV^{1/2}$, $S_0 = \langle \Gamma_n^o \rangle_{ev.} / \langle D \rangle_{ev.}$ = 1.237 x 10^{-4} $eV^{1/2}$.

The evaluated errors of <D> and $\langle \Gamma_n^o \rangle$ are essentially statistical and depend on the finiteness of sampling.

We give the average values of fission widths: $\langle \Gamma_f \rangle$ = (46.0 ± 10.0) meV, $\langle \Gamma_f \rangle_{min}$ = (5.1 ± 1.5) meV. The meaning of $\langle \Gamma_f \rangle_{min}$ and the method of obtaining $\langle \Gamma_f \rangle$ are described in detail in section 2. Here we only note that to obtain $\langle \Gamma_f \rangle$ we have to average the fission widths over an energy interval which is a multiple of the interval of structure in the fission cross-section (D ~ 1 keV). The selection of the average radiation width $\langle \Gamma_f \rangle$ = (34.0 ± 6.1) meV is described in section 1.2.

2. NEUTRON CROSS-SECTIONS IN THE UNRESOLVED RESONANCE REGION FROM 0.5 TO 150 keV

In the present evaluation the unresolved resonance region was limited to 0.5-150 keV. The lower boundary was determined by the length of the region of resolved resonances which were experimentally reliable. The upper boundary was determined by the fact that the value of strength function S_2 was known and that it was impossible to take correct account of the competition of inelastic scattering at the second excited level (145.96 keV, 4^+).

2.1. Experimental data in the unresolved resonance region

In the interval of unresolved resonance energies we can make use of the experimental data [6] for the total cross-section in the narrow region up to 6.5 keV, of the capture cross-section [10] and also of the fission cross-section data from Refs [9, 16, 20]. The averaged values of cross-sections from these studies are given in Tables 2.1-2.4.

2.2. Evaluated average resonance parameters

The average level spacings and neutron widths were obtained by the standard procudure [21] from $\langle D \rangle_{ev.}$ in the region of resolved resonances and strength functions S^{0+} and S_1^{0+} for the ground state and S_0^{2+} and S_1^{2+} for the first excited state of the nucleus. Strength function $S_0^{0+} = 1.237 \times 10^{-4}$ $(eV)^{-1/2}$ is equal to that evaluated from the resolved resonance region. The other strength functions were obtained from calculations by the generalized optical model with potential parameters described in section 4 and are equal to $S_1^{0+} = 2.12 \times 10^{-4}$ $(eV)^{-1/2}$, $S_0^{2+} = 1.24 \times 10^{-4}$ $(eV)^{-1/2}$, $S_1^{2+} = 2.08 \times 10^{-4}$ $(eV)^{-1/2}$. Strength functions S_2 are taken to be equal to S_0. The evaluated values of the average level spacings and the average neutron widths are given in Tables 2.5-2.7.

The experimental data on fission cross-sections [9, 11, 20] showed an intermediate structure resolved up to ~ 10 keV with a width of ~ 0.1-0.2 keV and an average distance of about 1 keV between states. This

structure may be associated with the existence of quasi-stationary states of the fissile ^{239}Pu nucleus in the second well [22]. The fission penetration curves in this case become envelopes of fission resonances in the second well. Considering that these resonances can be described by the Breit-Wigner law, and following Ref. [23], we obtain the distribution of fission widths:

$$\varphi(x)dx = \frac{dx}{\pi x}(x-x_{min})^{-1/2}(x_{max}-x)^{-1/2},$$

where $x = \Gamma_f/\langle\Gamma_f\rangle$; $x_{min} = \Gamma_{fmin}/\langle\Gamma_f\rangle$; $x_{max} = \Gamma_{max}/\langle\Gamma_f\rangle$

with condition $\langle\Gamma_f\rangle = \sqrt{\Gamma_{fmax}\Gamma_{fmin}}$.

Quantities Γ_{fmin} and Γ_{fmax} are determined by the minimum and maximum penetrations. Then,

$$\langle\Gamma_f\rangle = \frac{\langle D\rangle \cdot \nu_f}{2\pi} \cdot \frac{P_A P_B}{1-(1-P_A)(1-P_B)},$$

$$x_{max} = \frac{1}{x_{min}} = \frac{1+\sqrt{(1-P_A)(1-P_B)}}{1-\sqrt{(1-P_A)(1-P_B)}},$$

where P_A and P_B are the penetrations of the first and second humps of the double-humped fission barrier calculated by the Hill-Wheeler formula

$$P_{A,B} = 1/\left\{1+\exp\left[\frac{2\pi(E_{fA,B}-E)}{\hbar\omega_{A,B}}\right]\right\}.$$

The fission barrier parameters are chosen in the following manner. The curvature of the first hump $\hbar\omega_A$ = 1 MeV was determined from the slope of the curve of the fission cross-section in the near-threshold region, and curvature $\hbar\omega_b$ = 0.6 MeV was taken from the systematics. The values of thresholds E_{fA} = 0.652 MeV and E_{fB} = 0.06 MeV were determined from the average value of fission width and its fluctuations range x_{max} in the resolved resonance region. We consider that, apart from the given distribution, the fission widths are subjected to local fluctuations described by the χ^2-distribution with the number of degrees of freedom ν_f, taken to be equal to 2J + 1 (J is the spin of the compound nucleus in the calculations). The evaluated values of the average fission widths and factor x_{max} are given in Table 2.8.

The average radiative capture width $\langle\Gamma_\gamma\rangle$ = 34 meV for the different channels was taken to be identical since the dependence of

$\langle\Gamma_\gamma\rangle$ on spin J predicted by the cascade photon emission model is much smaller than the experimental uncertainty of this value. Moreover, in the calculations it was assumed that $\langle\Gamma_\gamma\rangle$ was not dependent on energy since the increase in the total width of photon emission with rise in energy is compensated by the increase in the width of the (n,γf) process.

2.3. Average cross-sections in the unresolved resonance region

The average resonance parameters described in the preceding section were used to calculate the average cross-sections. The fission widths undergo fluctuations caused not only by the χ^2-distribution but also by the double-humped fission barrier structure. Therefore, $\left\langle\frac{\Gamma_{nf}\Gamma_{nf}}{\Gamma_n}\right\rangle$ was not calculated but was determined by averaging the values of $\frac{\Gamma_{nf}\Gamma_{nf}}{\Gamma_n}$ obtained by random selection of the corresponding distributions. Here special steps were taken to reduce the error associated with the finiteness of sampling for each channel so that it was possible to calculate the average cross-sections with an accuracy of more than 1% for a reasonable expenditure of computer time. The evaluated average resonance parameters and cross-sections smoothly depend on energy since the structure in the experimental data was not measured with sufficient reliability.

The evaluated average cross-sections are compared with the experimental data and evaluations of other authors in Figs 2.1-2.3. As will be seen from Fig. 2.1, our evaluated data for σ_t are, on an average, 6×10^{-28} m^2 lower than the measurement results of Ref. [6], i.e. there is the same difference as in the resolved resonance region, which was discussed in the preceding section. Comparison with the evaluations of other authors shows the degree of their confidence in the data of Ref. [6]: the ENDF/B-V evaluation [18] was made on the basis of experiment, while Derrien [17] renormalized the results of Ref. [6] and his evaluation agrees with ours.

The evaluated fission cross-section of the present study (Fig.2.2) shows satisfactory agreement with the available experimental data but is closer to the measurements of Ref. [16]. The evaluated data of Ref. [17] and

ENDF/B-V are based mainly on the measurements of Ref. [9] and are somewhat higher than our evaluation.

The difference between the experimental [10] and evaluated values is as much as ~ 40% in the region up to ~ 40 keV, and the agreement between calculation and experiment cannot be improved by any reasonable change of the parameters. We recall that the same difficulties occur when we try to describe the dips of experimental data in the resolved resonance region. The data for $\sigma_{n\gamma}$ [10] evidently contain neglected experimental errors.

Calculations were performed also of $\sigma_{n\gamma}$ and σ_{nf} without taking into account fluctuations of fission widths due to the double-humped fission barrier structure (dashed curves in Figs 2.2 and 2.3). It will be seen that such calculations describe the experimental data for σ_{nf} much less satisfactorily.

3. EVALUATED FISSION CROSS-SECTIONS FOR ^{238}Pu IN THE FAST ENERGY REGION (0.15-20 MeV)

The ^{238}Pu nuclei have a high alpha-activity, which substantially complicates experimental determination of the fission cross-section. It is difficult to evaluate this cross-section because there is not a single experimental study with sufficiently reliable data covering the entire range of fast neutron energies.

3.1. Experimental data on $\sigma_{nf}(^{238}Pu)$ in the fast energy region

In the evaluation of σ_{nf} the following experimental data were used:

1. Ermagambetov and Smirenkin [16] measured the $\sigma_{nf}(^{238}Pu)/\sigma_{nf}(^{235}U)$ ratio in the 2.5 keV-2.4 MeV region with an accuracy of ~ 10-5%.
2. In Ref. [24] the same authors determined the $\sigma_{nf}(^{238}Pu)/\sigma_{nf}(^{235}U)$ ratio at four points (0.5-1.5 MeV) and the $\sigma_{nf}(^{238}Pu)/\sigma_{nf}(^{238}U)$ ratio in the 1.5-5.6 MeV and 13-16.0 MeV intervals with an accuracy of ~ 5%.

3. Fomushkin and Gutnikova [25] measured the $\sigma_{nf}(^{238}Pu)/\sigma_{nf}(^{235}U)$ ratio in the 1-3.6 MeV region with an accuracy of ~ 5%.

4. Barton and Koonts [26] determined the $\sigma_{nf}(^{238}Pu)/\sigma_{nf}(^{235}U)$ ratio at four points (1, 1.5, 3 and 14.9 MeV) with an accuracy of ~ 5%.

5. Budtz-Jorgensen and co-workers [11] measured the $\sigma_{nf}(^{238}Pu)/\sigma_{nf}(^{235}U)$ ratio in the region up to 10 MeV with an accuracy of ~ 4%.

6. Aleksandrov and co-workers [27] determined the $\sigma_{nf}(^{238}Pu)/\sigma_{nf}(^{238}U)$ and $\sigma_{nf}(^{238}Pu)/\sigma_{nf}(^{235}U)$ ratios at 2.9 MeV.

7. Fomuskin and co-workers [28] measured the $\sigma_{nf}(^{238}Pu)/\sigma_{nf}(^{238}U)$ ratio at 14.5 MeV.

There are also the data of Refs [9, 20] in which the $\sigma_{nf}(^{238}Pu)/\sigma_{nf}(^{235}U)$ ratio was measured in the region up to several megaelectron-volts. It is difficult to judge the accuracy of results in this region. The data of Ref. [29] are systematically higher than those of other authors because an erroneous value was taken for σ_{nf} at 0.72 MeV.

3.2. Evaluation of fission cross-section $\sigma_{nf}(^{238}Pu)$

All the available data for $\sigma_{nf}(^{238}Pu)$ are measurements mainly of its ratios to $\sigma_{nf}(^{235}U)$ and $\sigma_{nf}(^{288}U)$. Therefore, we recalculated these data into absolute cross-sections, using as standard the values of σ_{nf} from Ref. [30] for ^{235}U and Ref. [31] for ^{238}U (Figs 3.1-3.3).

In the threshold region (0.15-1 MeV) the data of Refs [16, 24, 25], which were obtained with track detectors insensitive to alpha particles, agree satisfactorily with the results of Ref. [11], where an ionization chamber with suppressed alpha background effect was used. The data of Ref. [29] given in Figs 3.1 and 3.2 were obtained by renormalizing the values of this study with a normalization factor of 0.719 determined over the 570-785 keV interval. The

evaluated curve for σ_{nf} in the threshold region (Fig. 3.1) is drawn along the experimental data with allowance for these errors.

In the region of the first "plateau" (Fig. 3.2) the situation is somewhat more complicated. Although most experimental values agree with each other within experimental errors, the data of Ref. [11] are characterized by a substantial scatter and those of Ref. [25] for $E \simeq 2.5$-3.6 MeV are systematically higher than the results of the other authors so that it is not possible reliably to determine the slope of the first "plateau" of the σ_{nf} curve in the region above ~ 3 MeV. In view of this, in order to evaluate the energy dependence of σ_{nf} we used the results of analysis of experimental data for the major even-even plutonium isotopes, whose neutron fission cross-sections have been studied in much greater detail. We know [32, 33] that the fission cross-section undergoes a virtually linear decrease with rise in neutron energy from ~ 2 MeV to the threshold of the (n,n'f) reaction. The slope of this dependence on the value of A, when we go over to the minor isotopes, decreases almost linearly and, for ^{238}Pu(n,f), is about 0.05×10^{-28} m^2/MeV. The evaluated curve of $\sigma_{nf}(^{238}Pu)$, thus drawn, is not inconsistent with the existing experimental data in the region up to the threshold of the (n,n'f) reaction.

In the region of the (n,n'f) reaction threshold the fission cross-section has been measured only in Ref. [11] although here, too, the scatter of data is large. Moreover, the high value of the cross-section ($\sim 2.8 \times 10^{-28}$ m^2, at the maximum points $\sim 3 \times 10^{-28}$ m^2) is difficult to interpret, considering both the compound nucleus formation cross-section (see Fig.3.3) and the experimental data for the major even-even isotopes of plutonium (A = 240-244). The systematics of the cross-sections at the constant excitation energy for isotopes (Z = 94) and isotopes (N = 144) [34] and the theoretical calculation of the fission cross-sections by the statistical cascade theory [35] lead to the same conclusion.

As a result, the evaluation of the fission cross-section in the region from the (n,n'f) reaction threshold to 20 MeV was based on calculations by the statistical cascade model. It was assumed here that the proportion of pre equilibrium emission of neutrons in the primary neutron spectrum, obtained in the case of the U isotopes, varies negligibly from one nucleus to another and can be used for the ^{238}Pu target nucleus. The fission barrier parameters of the ^{238}Pu and ^{237}Pu compound nuclei, which undergo fission in reactions ^{239}Pu(n,xnf), x = 1, 2, were chosen with allowance for the charged-particle fission data [36]. The fission cross-section, thus obtained, agrees satisfactorily at E_n = 14-15 MeV with the available experimental data. In the region from the (n,n'f) reaction threshold to ~ 10 MeV the curve of the evaluated cross-section σ_{nf} passes along the lower edge of experimental data [11] but fully agrees with the phenomenological evaluation of the fission cross-section [34] on the second "plateau". It is not possible to achieve a better agreement between the evaluated fission cross-section curve and the data of Ref. [11] in the 6-10 MeV region within the framework of the approach described here since this would lead to an unjustified increase in the compound nucleus formation cross-section. It can be concluded that the data of Ref. [11] in the region of the (n,n'f) reaction threshold are on the higher side and do not correspond to the isotopic dependence of σ_{nf} on the second "plateau" for the even-even isotopes of plutonium.

We note that the neutron transmission coefficients T&j(E) needed for the calculations were obtained from the generalized optical model calculations with potential parameters whose selection is described in section 4.

The evaluated values of the $\sigma_{nf}(^{238}Pu)/\sigma_{nf}(^{235}U)$ ratios and their errors are given in Table 3.1. The errors are taken on the basis of the actual scatter of experimental data.

From a comparison of the different evaluations (see Figs 3.1-3.3) it will be seen that in the region up to ~ 1 MeV the evaluations of ENDF/B-V [18] and Derrien [17] are somewhat higher than the data of the

present work since they are based to a great extent on the measurements of Refs [9] and [20]. However, the data of these studies are not sufficiently reliable in the high region. In the 1-3 MeV region the evaluation of the present work agrees satisfactorily with Ref. [17], while that of ENDF/B-V is somewhat lower. At 3-10 MeV our evaluation lies between the evaluations under discussion. At 14 MeV all three evaluations show satisfactory agreement. At higher energies the ENDF/B-V evaluation is substantially higher than the results of the present work. However, such a large value of the fission cross-section cannot be explained on the basis of our concepts about the compound nucleus formation cross-section.

4. CROSS-SECTIONS FOR INTERACTION OF FAST NEUTRONS (0.15-20 MeV) WITH THE ^{238}Pu NUCLEUS

No experimental data exist on the cross-sections for fast neutron interaction with the ^{238}Pu nucleus in the 0.15-20 MeV region, except for data on the fission cross-section and three points for σ_{nf} [10]. Therefore, the evaluation of the neutron cross-sections for these energies was performed on the basis of calculations by the generalized optical and statistical models.

4.1. Optical cross-sections

The optical cross-sections form the basis of evaluation of all types of cross-section in the fast region since they determine the total, direct-interaction and compound nucleus formation cross-sections and also the neutron transmission coefficients needed in all statistical calculations. The COUPLE program [37], based on the coupled-channel method, was used to calculate the optical cross-sections. The parameters of the generalized optical model potential for nuclei of the actinide group were obtained in Ref. [38]. To use this potential for a specific nucleus, we only need to know its deformation parameters β_2 and β_4. Microscopic calculations of these parameters

[39, 40] do not unambiguously determine the values of β_2 and β_4 but satisfactorily predict their isotopic dependence. Using this dependence and the values for ^{238}Pu chosen in Ref. [38], we were able to obtain β_2 and β_4 for the ^{238}Pu. The quadrupole deformation parameter β_2 was then refined by fitting the strength function S_0 calculated by the general optical model to its value evaluated from the resolved resonance region. This fully determined the parameters of the generalized optical model potential for the ^{238}Pu nucleus:

$$V_R = \begin{cases} 46{,}15 - 0{,}3E, & E \leqslant 10 \text{ MeV} \quad r_1 = 1{,}256, \\ 43{,}15, & E > 10 \text{ MeV} \quad a_1 = 0{,}626; \end{cases}$$

$$W_D = \begin{cases} 3{,}12 + 0{,}4E, & E \leqslant 10 \text{ MeV} \quad r_2 = 1{,}260, \\ 7{,}12, & E > 10 \text{ MeV}, \quad a_2 = 0{,}555 + 0{,}0045E; \end{cases}$$

$$V_{S_0} = 7{,}5\,, \qquad \beta_2 = 0{,}218\,, \qquad \beta_4 = 0{,}087.$$

The calculations were performed with allowance for the coupling of the first three levels of the main rotational band of ^{238}Pu.

4.2. Calculations by the statistical model

The cross-sections for compound processes were calculated by the statistical model of nuclear reactions. The level scheme used for the ^{238}Pu nucleus is shown in Table 2. At energies above the last level there is a substantial gap of missing levels; therefore, the level density was taken in the form of a continuous dependence. For incident neutron energies below 1.07 MeV we performed the calculations, taking into account corrections for width fluctuation by the Hauser-Feschbach-Moldauer formalism. For higher energies such fluctuations were taken into account within the framework of the formalism of Tepel and co-workers.

The continuous level density in the neutron and fission channels was determined by the relations of the superfluid model. At low excitation energies it is smoothly matched with the density which follows from the constant temperature model. The specific relations of the adopted level density model are described in greater detail in Ref. [21], and the model parameters are taken from the systematics of Ref. [41].

Radiative capture transmissions were calculated by the cascade photon emission model. The parameters of the photo-absorption curve needed for the purpose were taken from Ref. [41]. The calculated value of the radiative capture width was normalized to the experimental value of $\langle\Gamma_\gamma\rangle$ = 34 meV from the resolved resonance region. The cross-sections for reactions with preliminary neutron emission (n,n'f), (n,2n), (n,2nf) etc. were calculated by the STAPRE program [42]. The evaluated values of cross-sections σ_t, σ_{nn}, $\sigma_{nn'}$, $\sigma_{n\gamma}$, σ_{nf}, σ_{n2n} and σ_{n3n} are given in Table 4.1 and the evaluated discrete-level and continuous-spectrum excitation cross-sections in Table 4.2.

4.3. Comparison of the different evaluations

In Figs 4.1-4.3 we compare the different types of cross-section of the present work with the evaluations of ENDF/B-V [18] and Derrien [17]. As will be seen from Fig. 4.1, our evaluation and the ENDF/B-V data of σ_t and σ_{nn} agree satisfactorily in the region up to ~ 0.5 MeV. For higher energies the differences are quite noticeable and are explained by the fact that in evaluation [18] these cross-sections were obtained from calculations by the spherical optical model. The evaluation of σ_t and σ_{nn} in the present work, which is based on calculations by the coupled-channel method with a potential describing the cross-sections for the actinide group, agrees satisfactorily with Derrien's evaluation [17] and appears to be preferable.

The considerable differences in the values of evaluated inelastic scattering cross-sections reflect the differences in the physical approaches used. The ENDF/B-V evaluation in the region up to ~ 1.5 MeV lies below the data of our evaluation and of Derrien [17] since it does not take into account the contribution of the direct excitation of levels. At higher energies the differences become even more considerable as the mechanism of pre-equilibrium neutron emission is also not taken into consideration. The agreement with Derrien's evaluation [17] is sufficiently good, except for energies of about 10 MeV, owing evidently to the difference of approaches in describing the pre-equilibrium neutron emission.

The differences in the evaluated values of the radiative capture cross-section (Fig. 4.2) are substantial. In the region up to 300 keV, evaluation [18] is higher than the others since it follows experimental data [10], which are not regarded as sufficently reliable in the present work and in evaluation [17]. As a consequence, in the region up to ~ 5 MeV the ENDF/B V evaluation of $\sigma_{n\gamma}$ is systematically higher than our data. The differences between the present evaluation of $\sigma_{n\gamma}$ and Derrien's evaluation [17] are evidently due to differences in the energy dependence of the radiative capture width and to making allowance for the competition of the $(n,\gamma f)$ process.

The greatest differences between the data of the different authors are observed in the evaluated values of the (n,2n) and (n,3n) reaction cross-sections (see Fig. 4.3). As a result, it is advisable to discuss the evaluations of the reaction cross-sections for other plutonium and uranium isotopes. This is all the more necessary because the ^{238}Pu (n,3n) ^{236}Pu reaction leads to the production of ^{232}U, which substantially complicates the external fuel cycle technology.

Figures 4.4 and 4.5 show the available evaluations of the maximum values of cross-sections σ_{n2n} and σ_{n3n} for uranium and plutonium isotopes. Since the isotopic dependence of the compound nucleus formation cross-sections in the energy region considered is weak, it can be concluded that changes in the (n,2n) and (n,3n) reaction cross-sections at the maximum are determined by changes in the fissility of nuclei [43]. For all uranium and plutonium isotopes, the fissility increases monotonically with decrease in the relative atomic mass and, therefore, the (n,2n) and (n,3n) reaction cross-sections in their case should decrease monotonically. In the ENDF/B-V evaluations this dependence breaks down for the uranium and plutonium isotopes, indicating inconsistency of the evaluations for the different isotopes. In the consistent theoretical calculations, however, the monotonic isotopic increase of cross-sections σ_{n2n} and σ_{n3n} is fully reproducible

(Fig. 4.4 and 4.5). Therefore, the present evaluation of the (n,2n) and (n,3n) cross-sections is sufficiently reliable.

5. EVALUATION OF THE CHARACTERISTICS OF SECONDARY NEUTRONS AND $\bar{\nu}$ FOR ^{238}Pu

Experimental data on secondary neutron energy and angular distributions and on $\bar{\nu}$ for ^{238}Pu are totally lacking. Their evaluation was therefore based on theoretical calculations and systematics.

5.1. Evaluation of secondary neutron energy spectra

The secondary neutron energy distributions were obtained from calculations by the statistical model with allowance for the likelihood of pre-equilibrium primary neutron emission and competition of fission and other possible processes at the successive stages of neutron emission. The calculation method was described in detail in a previous study [21]. Owing to the large volume of data, the spectrum tables are not given; they can be obtained from the complete ^{238}Pu file transmitted to the Nuclear Data Centre.

The fission neutron spectrum is taken in the form of a Maxwellian distribution. The temperature of this spectrum during thermal neutron fission is taken as equal to the experimental value T_M = (1.35 ± 0.04) MeV [44]. The dependence of T_M on energy follows from the systematics:

$$T_M = a + b[1 + \bar{\nu}(E)]^{1/2},$$

where $\bar{\nu}(E) = [\nu_t(E)\cdot\sigma_{nF}(E) - \sigma_{n,n'f}(E) - 2\sigma_{n,2nf}(E)]/\sigma_{nF}(E)$.

Coefficients a and b were so chosen as to satisfy the value of T_M at the thermal point and to describe the rise in E = 3/2 T by ~ 1% with increase in excitation energy by 1 MeV: a = 0.873 and b = 242. The evaluated values of the fission spectrum temperature are given in Table 5.1.

5.2. Value of $\bar{\nu}_t$ for ^{238}Pu

The value of $\bar{\nu}_p$ was not evaluated. As evaluated data we took those from Ref. [45], where they had been obtained in accordance with the

systematics of $\bar{\nu}_p$ for the neighbouring fissile nuclei. The dependence of $\bar{\nu}_d$ was chosen with consideration of the systematics and is ν_d(E = 10^{-5}-5 MeV) = 0.045, ν_d (E = 9-20 MeV) = 0.027. It decreases linearly between the boundaries of these regions. The evaluated values of $\bar{\nu}_t$ and $\bar{\nu}_p$ are given in Table 5.2.

The value of $\bar{\nu}_p^{sp}$ (^{252}Cf) = 3.757 ± 0.005 was used as the standard. The error of the evaluated values of $\bar{\nu}_t$ was approximately 3%.

5.3. Angular distributions of scattered neutrons

The angular distributions of elastically scattered neutrons and those scattered on the first two levels of the ^{238}Pu nucleus were calculated by the generalized optical model. They take into account the isotropic contribution of these compound processes.

The angular distributions of neutrons scattered on the other levels of the nucleus and emitted in other reactions are taken to be isotropic.

CONCLUSION

Available experimental data for ^{238}Pu being limited, it was necessary to make extensive use of theoretical models for the evaluation. The reliability of the evaluated data obtained is determined to a large extent by the correctness of these models and of the systematics of their parameters.

The models and systematics used for evaluation of ^{238}Pu were pre-validated on the basis of available experimental data for ^{235}U, ^{238}U and ^{239}Pu, and this assures us of the reliability of the evaluated data obtained.

The full system of evaluated neutron data for ^{238}Pu in the 10^{-5}-20 MeV region, presented in this study, has been transmitted in the ENDF/B format to the Nuclear Data Centre of the USSR State Committee on the Utilization of Atomic Energy.

REFERENCES

1. Barre J.Y., Bouchard J. Importance of Transactinide Nuclear Data for the Physics of Fast and Thermal Reactor Cores // Transactinium Isotope Nuclear Data: Proc. of an Advisory Group Meeting, Karlsruhe, 1975. - Vienna: IAEA, 1976. - V. 1.- P. 113-137.
2. Bouchard J. Comprehensive Review of TND Requirement for U and Pu - Fueled Thermal and Fast Reactors, and Their Associated Fuel Cycles // Transactinium Isotope Nuclear Data: Pros. of the Second Advisory Group Meeting, Cadarache, 1979.- Vienna: IAEA, 1980. - P. 1-21.
3. Howerton R.J. Thresholds of Nuclear Reactions Induced by
4. Kravtsov, V.A., Masses of Atoms and Binding Energies of Nuclei, Atomizdat, Moscow (1974) 344 pp (in Russian).
5. Lederer C.M., Shirley V.S. Tables of Isotopes. 7-th ed. - N.Y.: J.Whiley and Sons Inc., 1978.
6. Neutron Total and Absorption Cross Sections of ^{238}Pu / T.E.Young, F.B.Simpson, J.R.Berreth, M.S.Coops // Nucl.Sci. Eng. - 1967. - V. 30. - P. 355-361.
7. Gerasimov, V.F., "Cross-sections for ^{238}Pu and ^{241}Am fission induced by monochromatic resonance neutrons", Yad. Fiz. 4 5 (1966) 985-922.
8. Neutron-Induced Resonance Fission Cross Sections of ^{238}Pu / W.F.Stubbins, C.D.Bowman, G.F.Auchampaugh, M.S.Coops // Phys.Rev. - 1967. - V. 154. - P. 1111-1115.
9. Silbert M.G., Moat A., Young T.E. Fission Cross Section of Plutinium-238 // Nucl.Sci.Eng. - 1973. - V. 52. - P. 176-186.
10. Silbert M.G., Berreth J.R. Neutron Capture Cross Section of Plutonium-238: Determination of Resonance Parameters // Nucl.Sci.Eng. - 1973. - V. 52. - P. 187-200.
11. Budtz-Jorgensen C., Knitter H.H., Smith D.L. Neutron Induced Fission Cross Section of ^{238}Pu in the Energy Range from 5 eV to 10 MeV // Nuclear Data for Science and Technology: Proc. of Int.Conf. - Antwerpen, 1982. - P. 206-210.
12. Bruehlman R.J., Bentley W.C., Hyde E.K. ANL-4215, 1948,- P. 17
13. Butler J.P., Lounbury M., Merritt J.S. The Neutron Capture Cross Sections of ^{238}Pu, ^{242}Pu and ^{243}Am in the Thermal and Epicadmium Regions // Canadian Journ. of Physics. - 1957.- V. 35. - P. 147-154.
14. Thermal Neutron Fission Cross Sections for Isotopes of Plutonium, Americium and Curium / E.K.Hulet, R.W.Hoff, H.R. Bowman, M.C.Michel // Phys.Rev. - 1957. - V. 107. - P. 1294-1296.
15. Radiochemical Methods Applied to the Determination of Cross Sections of Reactor Interest / T.A.Eastwood, A.P.Baerg, C.B.Bigham et.al. // Proc. of the Sec. United Nations Int.Conf. on the Peaceful Uses of Atomic Energy. - Geneva, 1958. - V. 16. - P. 54-63.
16. Ermagambetov, S.B., Smirenkin, G.N., "Neutron-induced sub-barrier fission of ^{238}Pu", At. Ehnerg. 29 (1970) 422-424.
17. Derrien H. Evaluation of ^{238}Pu Neutron Cross Sections in the Energy Range 10^{-5} eV to 14 MeV. - INDC(FR)-57/L, 1982.- 38 p.
18. Kinsey R. ENDF/B Summary Documentation. - BNL-17541(ENDF-201). - Brookhaven, 1979.

19. Porodzinskij, Yu.V., Sukhovitskij, E.Sh., "A method of determining average neutron widths and level spacings with allowance for the finite resolution of experimental apparatus", Vestsi Akad. Navuk BSSR, Ser. Fiz.-Ehnerg. Navuk 3 (1986) 19-23.

20. Drake D.M. et.al. Fission Cross Sections from Pommard.- Report LA-4420, 1970. - P. 101-122.

21. Klepatskij, A.B., Kon'shin, V.A., Maslov, V.M., et al., Evaluated Neutron Data for ^{236}U, Rep. No. 2, Inst. of Nucl. Power, Byelorussian Acad. of Sc., Minsk (1987) 83 (in Russian).

22. Strutinsky V.M. Shell Effects in Nuclear Masses and Deformation Energies // Nucl.Phys. - 1967. - V. A95, N 2. - P. 420-442.

23. Gaj, E.V., Ignatynk, A.V., Rabotnov, N.S., Smirenkin, G.N., "Double-humped barrier and neutron fission of nuclei", Yad. Fiz. 10 (1969) 542-548.

24. Ermagambetov, S.B., Smirenkin, G.N., "Fast-neutron fission cross-section of ^{238}Pu", At. Ehnerg. 25 (1968) 527-529.

25. Fomushkin, Eh.F., Gutnikova, E.K., "Cross-sections and angular distributions of fragments during ^{238}Pu, ^{242}Pu and ^{241}Am fission induced by 0.45-3.6 MeV neutrons", Yad. Fiz. 10 (1969) 917-922.

26. Barton D.M., Koonts P.G. Neutron Induced Fission Cross Sections of ^{238}Pu // Phys. Rev. - 1967 - V. 162, N 4. - P. 1070-1076.

27. Aleksandrov, B.M., Solov'ev, S.M., Soloshenkov, P.S., et al. "Neutron fission of ^{241}Am, ^{238}, ^{240}, ^{241}Pu" in: Problems of Atomic Science and Technology, Ser. Nuclear Constants, No. 1 (50) (1985) 3-4 (in Russian).

28. Fomushin, Eh.F., Gutnikova, E.K., Zamyatin, Yu.S., et al., "The cross-sections and angular anisotropy of fragments during the fast neutron fission of some plutonium, americium and curium isotopes", Yad. Fiz. 5 (1967) 966-970.

29. Vorotnikov, P.E., Dubrovina, S.M., Otroshenko, S.A., et al. "Channel analysis of neutron fission of ^{238}Pu", Yad. Fiz. 3 (1966) 479-486.

30. Yankov G.B. The ^{235}U Fission Cross Section // Nuclear Data Standards for Nuclear Measurements. Techn.Rep.Series N 227.- Vienna: 1983. - P.39-45.

31. Smith A.B. The ^{238}U Fission Cross Section // Nuclear Data Standards for Nuclear Measurements. Techn.Rep.Series N 227.

32. Smirenkin, G.N., Fursov, B.N., "The dependence of the fission cross-sections of heavy nuclei on neutron energy in the "plateau" region in: Problems of Atomic Science and Technology, Ser. Nuclear Constants No. 2 (1985) 31-36 (in Russian).

33. Ignatyuk, A.V., Klepatskij, A.B., Maslov, V.M., Sukhovitskij, E.Sh., "Analysis of the neutron fission cross-sections of U and Pu isotopes in the first "plateau" region, Yad. Fiz. 42 (1985) 569-577.

34. Behrens J.W. Inferred ^{238}Pu (n,f) Cross Section in the MeV Range // Trans.Amer.Nucl.Soc. - 1982. - V. 43. - P. 722-723.

35. Grudzevich, O.T., Ignatyuk, A.V., Maslov, V.M., Pashchenko, A.B., "A consistent description of the (n,n'f) and (n,xn) reaction cross-sections for transuranic nuclei" in: Neutron Physics: Proceedings of the 6th All-Union Conf. on Neutron Phys., Kiev, 2-6 October 1983, TzNIIatominform, Moscow, 2 (1983) 318-323 (in Russian).

36. Britt H.C., Wilhelmy J.B. Simulated (n,f) Cross Sections for Exotik Actinide Nuclei // NSE. -1979. -V.72.-P.222-229.

37. Antsipov, G.V., Bakhanovich, L.A., Benderskij, A.R., et al., "Evaluation of neutron cross-sections for ^{242}Pu in the 0.2-15.0 Mev region on the basis of experimental data and theoretical models" in: Evaluation of Nuclear Data for ^{242}Pu in the 10^{-5}eV-15 Mev Neutron Energy Region, Inst. of Heat and Mass Exch., Byel. Acad. Sc., Minsk (1979) 53-111 (in Russian).

38. Klepatskij, A.B., Kon'shin, V.A., Sukhovitskij, E.Sh., "The coupled-channel method and evaluation of neutron data for fissile nuclei", Vestsi Akad. Navuk BSSR, Ser. Fiz.-Ehnerg. Navuk, 2 (1984) 21-29.

39. Möller P., Nilsson S.G., Nix J.R. Calculated Ground-State Properties of Heavy Nuclei // Nucl.Phys. - 1974. - V. A229, N 2. - P. 292-319.

40. On the Nuclear Structure and Stability of Heaby and Super-heavy Elements / S.G.Nilsson, Ch.P.Tsang, A.Sobiczewsky et.al. // Nucl.Phys. - 1969. - V. A131, N 1. - P. 1-66.

41. Antsipov, G.V., Kon'shin, V.A., Maslov, V.M., "Level density and radiation widths of transactinides" in: Problems of Atomic Science and Technology, Ser. Nuclear Constants No. 3 (1985) 25-34 (in Russian).

42. Uhl M., Strohmaier B. Report IRK-76/01. - Vienna, 1976.

43. Ignatyuk, A.V., Maslov, V.M., "Consistent evaluation of the neutron cross-sections of curium-242, 243 and 244" in: Problems of Atomic Science and Technology, Ser. Nuclear Constants No. 4 (1986) 43-48 (in Russian).

44. Zamyatin, Yu.S., Kroshkin, N.I., Mel'nikov, A.K., Nefedov, V.N., "Measurement of the energy spectra and average number of prompt fission neutrons of actinide elements" (in Russian) in: Nuclear Data for Reactors (Proc. Helsinki 1970), IAEA, Vienna 2 (1970) 183-193.

45. Malinovskij, V.V., Tarasko, M.Z., Kuz'minov, B.D., "Evaluation of the energy dependence of the average number of prompt neutrons during the neutron fission of plutonium isotopes", At. Ehnerg. 58 6 (1985) 430-435.

Table 1. Values of energies Q and thresholds T for reactions of neutrons with the ^{238}Pu nucleus.

Reaction		Q, MeV	T, MeV
(n,γ)	^{239}Pu	-	-
(n,2n)	^{237}Pu	-6,998	7,028
(n,3n)	^{236}Pu	-I2,857	I2,9II
(n,4n)	^{235}Pu	-20,2I4	20,300
(n,p)	^{238}Np	-0,508	0,5I
(n,np)	^{237}Np	-5,995	6,02
(n,d)	^{237}Np	-3,764	3,78
(n,t)	^{236}Np	-4,I32	4,I5
(n,^{3}He)	^{236}U	-9,679	9,72
(n,^{4}He)	^{235}U	-	-I0,90

Table 1.1. Experimental and evaluated areas A under capture and fission resonances.

Resonance No.	E_0, eV	A_i, $10^{-2}\bar{\varepsilon}_m^2$·eV	A_Γ, $10^{-2}\bar{\varepsilon}_m^2$·eV	Ref.
I	2	3	4	5
I	2,84	I,2 ± 0,2	-	/6/
	2,9I	3,4 ± I,4	-	/7/
2	9,98	I2 ± I	-	/6/
	I0,06	I6 ± 2	-	/7/
	9,97	I3,8 ± I,3	-	/9/
3	I8,56	22 ± 2	-	/6/
	I8,70	29 ± 2	-	/7/
	I8,60	37,3 ± 5,6	790 ± I66	/8/
	I8,54	2I,I ± I,7	-	/9/
4	32,2	I,I ± 0,275	7,8 ± 4,68	/8/
5	36,6	0,4 ± 0,2	2,4 ± I,5	/8/
6	59,8	8,0	-	/7/
	59,8	I,7 ± 0,I87	86,2 ± 8,62	/8/
7	70,3	I0 ± I	-	/6/
	70,2	25 ± 4	-	/7/
	70,I	24,6 ± 2,5	II4 ± 23	/8/
	70,34	22,3 ± 3,0	-	/9/
	70,22	23,9I ± I,73	II4 ± 23	
8	77,7	0,30 ± 0,08	I,I ± 0,76	/8/
9	83,2	3I ± 3	-	/6/
	83,0	6I ± 6	-	/7/
	83,0	62,4 ± 4,4	600 ± 72	/8/
	84,32	46,9 ± 4,2	-	/9/
	83,0	55,66 ± 2,7I	600 ± 72	
I0	96,2	0,30 ± 0,I5	2,I ± I,3	/8/
II	99,6	I,4 ± 0,28	9,3 ± 2,8	/8/
I2	II0,0	35 ± I2	-	/7/
	II0,I	I9,7 ± I,6	I63 ± 29,3	/8/
	II0,3	24,3 ± 3,I	-	/9/
	II0,2	20,87 ± I,4I	I63 ± 29,3	
I3	III,2	0,4 ± 0,2	4,5 ± 2,52	/8/

Table 1.1. (cont.)

1	2	3	4	5
I4	II4,0	42 ± 8	-	/7/
	II3,6	46,8 ± 3,7	290 ± 34,8	/8/
	II3,8	47,3 ± 3,8	-	
	II3,7	46,54 ± 2,52	290 ± 34,8	
I5	II9	38 ± II	-	/7/
	II8,6	25,0 ± 2,0	550 ± 60,5	/8/
	II8,9	20,9 ± 3,9	-	/9/
	II8,75	24,50 ± I,7,	550 ± 60,5	
I6	I22	II2 ± I9	-	/7/
	I22,4	II9 ± 9,6	470 ± 65, 8	/8/
	I22,7	II3,4 ± 5,8	-	/9/
	I22,55	II4,7I ± 4,80	470 ± 65,8	
I7	I29	0,2 ± 0,I	7,0 ± 5,46	/8/
I8	I32,4	3,5 ± 0,42	22 ± 5,3	/8/
I9	I39,7	I2,4 ± I,I2	66 ± 8,6	/8/
20	I5I	I07 ± I0	-	/7/
	I5I,I	I02 ± 9	380 ± 53,2	/8/
	I5I,6	93,6 ± 5,8	-	/9/
	I5I,35	98,I6 ± 4,38	380 ± 53,2	
2I	I65	I,3 ± 0,2	4,I ± 2,42	
22	I7I,0	I0,0 ± 0,9	470 ± 47	
23	I79	I45 ± 28	-	/7/
	I76,8	33,5 ± 2,7	26 ± 8,32	/8/
	I76,9	30,0 ± 4,7		
	I76,9	32,63 ± 2,34	26 ± 8,32	
24	I82,9	65,5 ± 5,2	3I0 ± 40,3	/8/
	I82,9	57,9 ± 5,5	-	/9/
	I82,9	6I,9I ± 3,78	3I0 ± 40,3	
25	I9I	224 ± 36	-	/7/
	I92,5	240 ± I7	63 ± 48,5	/8/
	I92,5	2I6 ± 8,9	-	/9/
	I92,5	22I,82 ±7,70	63 ± 48,5	
26	203	5,3 ± 0,53	84 ± 9,2	/8/
27	2I4	I32 ± 20	-	/7/
	2I6	I03 ± 8,2	I54 ± 32,3	/8/
	2I6,I	97,2 ± 6,9	-	/9/
	2I6,I	99,60 ± 5,28	I54 ± 32,3	
28	22I	I4,0 ± I,4	400 ± 44	/8/
29	232	0,3 ± 0,08	I2,I ± 4,84	/8/
30	245	43,I ± 3,4	58 ± I8,6	/8/
	244,8	36,9 ± 7,4	-	/9/
	244,8	42,02 ± 3,09	58 ± I8,6	
3I	249	I78 ± 3I	-	/7/
	252	I36 ± II	8I ± 43,7	/8/
	25I,9	I20,4 ± 8,2	-	/9/
	25I,9	I25,97 ± 6,57	8I ± 43,7	
32	26I	0,7 ± 0,2I	3,3 ± 2,6I	/8/
33	280	468 ± I48	-	/7/
	285	372 ± 37	-	/8/
	285,7	309,9 ± I2,7	-	/9/
	285,7	3I7,44		
34	289	I33 ± I3	I90 ± 4I,8	/8/
	289,4	II4,8 ± 8,I	-	/9/
	289,4	II9,89 ± 6,87	I90 ± 4I,8	

Table 1.1. (cont.)

I	2	3	4	5
35	300	406 ± 28,4	I35 ± 83,7	/8/
	300,5	355,2 ± I3,5	-	/9/
	300,5	364,56 ± I2,I9	I35 ± 83,7	
36	305	66,9 ± 6,7	33 ± I5,8	/8/
	305,5	89,I ± 7,4		/9/
	305,5	76,90 ± 4,97	33 ± I5,8	
37	3I2,4	73,4 ± 8,2	-	/9/
38	320	58,0 ± 4,I	360 ± 43,2	/8/
	320,7	I00,5 ± 8,I	-	/9/
	320,7	66,67 ± 3,66	360 ± 43,2	
39	327	67,4 ± 4,7	I55 ± 26,4	/8/
	326,9	60,2 ± 7,2	-	/9/
	326,9	67,94 ± 3,94	I55 ± 26,4	
40	337	27,5 ± 2,2	III ± I5,5	/8/
4I	36I	I,6 ± 0,48	7,3 ± 5,69	/8/
42	368	I5,3 ± I,53	I20 ± 2I,6	/8/
43	382	I,4 ± 0,49	2,7 ± 2,4	/8/
44	39I	7,8 ± I,I7	93 ± I5,8	/8/
45	408	8,4 ± I,26	II6 ± I2,8	/8/
46	4I9	I3I ± I0,5	I50 ± 5I	/8/
	420,9	I03,4 ± 8,8	-	/9/
	420,9	II4,79 ± 6,74	I50 ± 5I	
47	426	56,I ± 4,5	I69 ± 37,2	/8/
	427,8	45,5 ± 7,0	-	/9/
	427,8	53,00 ± 3,79	I69 ± 37,2	
48	448	38,4 ± 3,8	I8 ± II,9	/8/
	450,I	38,3 ± 6,5	-	/9/
	450,I	38,37 ± 3,28		
49	46I	33,0 ± 5,0	I67 ± 33,4	/8/
50	465	40,4 ± 6,I	204 ± 40,8	/8/
	464,0	I5,6 ± 4,5	-	
	464,0	24,34 ± 3,62	204 ± 40,8	
5I	473	7,8 ± I,2	II5 ± I8,4	/8/
	473,6	I0,9 ± 5,9	-	/9/
	473,6	7,92 ± I,I8	II5 ± I8,4	
52	496	I0,6 ± I,6	53 ± I0,6	/8/
	497,3	4,3 ± 4,2	-	/9/
	497,3	9,80 ± I,50	53 ± I0.6	

Table 1.2. Thermal cross-sections of ^{238}Pu.

Ref.	$\sigma_{n\gamma}$, 10^{-28} m^2	σ_{nf}, 10^{-28} m^2	Remarks
/I2/	455 ± 50	-	Activation measurements in reactor spectrum
/I3/	4I0 ± I4	-	Activation measurements above Cd-boundary. Result corrected in 1968
/I4/	520 ± 40	I8,4 ± 0,9	σ_γ - activation measurements in reactor spectrum σ_f - measurements by fission chamber in thermal flux
/I5/	-	I7,I ± 0,4	Fission chamber measurements in relation to ^{235}U in thermal spectrum
/I6/	-	I7,5 ± 0,7	Glass detector measurements in thermal spectrum

Table 1.3. Evaluated resonance parameters of ^{238}Pu.

Resonance No.	E_r, eV	Γ_n, meV	Γ_f, meV	Γ_γ, meV
I	2	3	4	5
-2	-I0,0	I2,0	4,5	34
-I	-0,4	0,439	I,0I8	34
I	2,885	0,0747 ± 0,003	I,2II ± 0,5	36,79±2
2	9,975	0,208 ± 0,0I3	6,778 ± 0,96	30,22±6
3	I8,562	3,489 ± 0,26	I,6I0 ± 0,27	37,39±6
4	32,2	0,070 ± 0,037	4,795 ± 3,23	34 ± 6,I
5	36,6	0,025 ± 0,0I3	5,667 ± 4,649	34
6	59,8	I,326 ± 0,I3I	0,67I ± 0,I57	34
7	70,22	2,496 ± 0,4I9	7,I3I ± I,906	34
8	77,7	0,026 ± 0,0I4	9,273 ± 7,067	34
9	83,0	20,532 ± 3,334	3,I54 ± 0,699	34
I0	96,2	0,056 ± 0,03I	4,857 ± 3,963	34
II	99,6	0,26I ± 0,069	5,II8 ± 2,067	34
I2	II0,2	5,649 ± 0,926	4,353 ± I,I46	34
I3	III,2	0,I33 ± 0,069	3,022 ± 2,333	34
I4	II3,7	I2,I65 ± I,500	5,456 ± I,2I7	34
I5	II8,75	3I,09I ± 6,6I0	I,5I5 ± 0,338	34
I6	I22,5	29,575 ± 5,777	8,298 ± I,924	34
I7	I29,0	0,277 ± 0,I72	0,97I ± 0,9I7	34
I8	I32,4	0,838 ± 0,I75	5,409 ± I,75I	34
I9	I39,7	2,849 ± 0,3I8	6,388 ± I,532	34
20	I5I,35	29,857 ± 5,805	8,783 ± 2,04I	34
2I	I65	0,2I8 ± 0,098	I0,78I ± 6,856	34
22	I7I	46,865 ± I3,8II	0,723 ± 0,203	34
23	I76,9	2,606 ± 0,386	42,670 ± I5,962	34
24	I82,9	27,79I ± 5,I79	6,790 ± I,564	34
25	I92,5	I4,588 ± 2,743	II9,7I2 ± 94,736	34
26	203	5,0I6 ± 0,538	7,I45 ± 0,500	34
27	2I6,I	I7,473 ± 2,7I2	2I,990 ± 6,I88	34
28	22I	60,383 ± 22,78I	I,I90 ± 0,278	34

Table 1.3. (cont.)

I	2	3	4	5
29	232	0,7I3 ± 0,279	0,843 ± 0,433	34
30	244,8	6,622 ± I,278	24,632 ± 9,238	34
3I	25I,9	I4,832 ± 3,479	52,876 ± 30,I99	34
32	26I	0,255 ± 0,I67	7,2I2 ± 6,237	34
33	285,7	27,I50 ± I,660	3370 ± 300	34
34	289,4	35,902 ± 8,230	2I,454 ± 6,22I	34
35	300,5	5I,374 ± I6,096	9I,8I5 ± 59,355	34
36	305,5	8,792 ± I,370	79,230 ± 40,849	34
37	3I2,4	4,88I ± 4,88I	97,75 ± 97,75	34
38	320,7	I90,I56 ± I95,08I	6,297 ± I,405	34
39	326,9	27,764 ± 5,I29	I4,903 ± 3,793	34
40	337	I5,48I ± 2,I72	8,423 ± 2,034	34
4I	36I	0,796 ± 0,5II	7,452 ± 6,367	34
42	368	I7,679 ± 3,509	4,335 ± I,I86	34
43	382	0,383 ± 0,229	I7,630 ± I7,I38	34
44	39I	I2,940 ± 2,324	2,852 ± 0,825	34
45	408	I8,638 ± 2,786	2,462 ± 0,638	34
46	420,9	49,35I ± I8,320	26,0I8 ± I0,126	34
47	427,8	47,753 ± I6,597	I0,663 ± 3,I26	34
48	450,I	6,544 ± I,459	72,477 ± 50,044	34
49	46I	49,8I3 ± I8,429	6,7I9 ± 2,075	34
50	464	79,588 ± 47,006	4,057 ± I,247	34
5I	473,6	23,I62 ± 4,97I	2,342 ± 0,662	34
52	497,3	9,350 ± I,698	6,287 ± I,946	34
53	5I0	2,5	3,4	34
54	5I8	25	I0	34

Table 1.4. Evaluated neutron cross-sections of ^{238}Pu at 0.0253 eV.

Ref.	σ_t, 10^{-28} m^2	$\sigma_{n\gamma}$, 10^{-28} m^2	σ_{nf}, 10^{-28} m^2	σ_{nn}, 10^{-28} m^2
Present work	583,33±I5,00	544,39±I5,20	I7,20±I,2C	2I,74±2,00
/I7/	583,75±I9,00	546,74±23,00	I7,I5±I,70	I9,86±I,20
ENDF/B-V /I8/	590,0	552,4	I7,0	20,60

Table 2. Level scheme of ^{238}Pu.

Level No.	E_i, keV	J^π	Level No.	E_i, keV	J^π
I	0,0	0^+	8	94I,5	0^+
2	44,08	2^+	9	962,77	I^-
3	145,96	4^+	I0	968,I	2^-
4	303,6	6^+	II	983,I	2^+
5	5I3,0	8^+	I2	985,46	2^-
6	605,I8	I^-	I3	I028,55	2^+
7	66I,43	3^-	I4	I069,95	3^+

Table 2.1. Averaged data on σ_t (^{238}Pu) from Ref. [6].

E, keV	σ_t, 10^{-28} m^2	E, keV	σ_t, 10^{-28} m^2	E, keV	σ_t, 10^{-28} m^2
0,5 - 0,6	24,5	I,4 - I,6	29,2	2,8 - 3,2	25,5
0,6 - 0,8	32 2	I,6 - I,8	30,5	3,2 - 3,6	26,I
0,8 - I,0	28,2	I,8 - 2,0	30,7	3,6 - 4,0	22,0
I,0 - I,2	26,4	2,0 - 2,4	3I,3	4,0 - 4,5	20,7
I,2 - I,4	28,3	2,4 - 2,8	25,9	4,5 - 5,5	20,4
				5,5 - 6,5	23,4

Table 2.2. Averaged data on σ_{nf} (^{238}Pu) from Ref. [9].

E, keV	σ_{nf}, 10^{-28} m^2	E, keV	σ_{nf}, 10^{-28} m^2	E, keV	σ_{nf}, 10^{-28} m^2
I - 2	I,36	I0 - I2	0,66	60 - 70	0,59
2 - 3	I,64	I2 - I4	0,93	70 - 80	0,59
3 - 4	I,04	I4 - I6	0,73	80 - 90	0,67
4 - 5	0,96	I6 - I8	0,86	90 - I00	0,70
5 - 6	I,57	I8 - 20	0,72	I00 - I20	0,64
6 - 7	I,20	20 - 25	0,88	I20 - I40	0,72
7 - 8	0,46	25 - 30	0,80	I40 - I60	0,74
8 - 9	I,07	30 - 40	0,82		
9 - I0	0,8I	50 - 60	0,69		

Table 2.3. Averaged data on $\sigma_{n\gamma}$ (^{238}Pu) from Ref. [10].

E, keV	$\sigma_{n\gamma}$, 10^{-28} m^2	E, keV	$\sigma_{n\gamma}$, 10^{-28} m^2	E, keV	$\sigma_{n\gamma}$, 10^{-28} m^2
I - I,2	6,27	7 - 8	I,90	40 - 50	0,72
I,2 - I,4	4,29	8 - 9	2,06	45 - 50	0,87
I,4 - I,6	3,59	9 - I0	2,I3	50 - 60	0,66
I,6 - I,8	3,7I	I0 - I2	2,06	60 - 70	0,5I
I,8 - 2,0	2,87	I2 - I4	2,08	70 - 80	0,63
2,0 - 2,4	4,5I	I4 - I6	I,83	80 - 90	0,49
2,4 - 2,8	3,78	I6 - I8	I,33	90 - I00	0,43
2,8 - 3,2	3,74	I8 - 20	I,37	I00 - I20	0,46
3,2 - 3,6	3,97	20 - 24	I,30	I20 - I40	0,36
3,6 - 4,0	3,38	24 - 28	I,24	I40 - I60	0,30
4 - 5	3,I4	28 - 32	0,93	I60 - I80	0,36
5 - 6	2,28	32 - 36	I,22		
6 - 7	2,07	36 - 40	0,93		

Table 2.4. Averaged data on σ_{nf} (^{238}Pu) from Ref. [20].

E, keV	σ_{nf}, 10^{-28} m^2	E, keV	σ_{nf}, 10^{-28} m^2
1 - 2	0,68	6 - 7	0,83
2 - 3	0,82	7 - 8	0,31
3 - 4	0,48	8 - 9	0,72
4 - 5	0,56	9 - 10	0,77
5 - 6	1,13		

Table 2.5. Evaluated average level spacings of the ^{239}Pu compound nucleus.

E*, keV	$\langle D\rangle_{1/2}$, eV	$\langle D\rangle_{3/2}$, eV	$\langle D\rangle_{5/2}$, eV
1	2	3	4
0,5	9,098	4,721	3, 349
1	9,089	4,717	3,346
1,5	9,081	4,713	3,343
2	9,072	4,708	3,340
2,5	9,064	4,704	3,337
3	9,055	4,699	3,334
4	9,038	4,691	3,327
6	9,005	4,673	3,315
8	8,971	4,656	3,303
10	8,938	4,639	3,290
12	8,905	4,621	3,278
14	8,872	4,604	3,266
16	8,839	4,587	3,254
20	8,774	4,553	3, 229
24	8,709	4,519	3,205
28	8,642	4,486	3, 18
32	8,580	4,452	3,158
36	8,517	4,420	3,134
40	8,454	4,387	3.111
45	8,376	4,346	3,082
50	8,299	4,306	3,054
60	8,146	4,227	2,997
70	7,997	4,149	2,942
80	7,850	4,073	2,888
90	7,706	3,998	2,835
100	7,565	3,925	2,783
110	7,427	3,853	2,731
120	7,291	3,782	2,681
130	7,158	3,713	2,632
140	7,027	3,645	2,584
150	6,899	3,579	2,536

* Energy is reckoned from neutron binding energy.

Table 2.6. Evaluated average neutron widths of ^{238}Pu.

E, keV	$\langle\Gamma_n^0\rangle_{1/2^+}$, meV	$\langle\Gamma_n^1\rangle_{1/2^-}$, meV	$\langle\Gamma_n^1\rangle_{3/2^-}$, meV	$\langle\Gamma_n^2\rangle_{3/2^+}$, meV	$\langle\Gamma_n^2\rangle_{5/2^-}$, meV
I	2	3	4	5	6
0,5	25,I64	0,073	0,038	0,0	0,0
I	35,554	0,206	0,I07	0,0	0,0
I,5	43,504	0,378	0,I96	0,0	0,0
2	50,I87	0,580	0,30I	0,0	0,0
2,5	56,059	0,809	0,420	0,0	0,0
3	6I,353	I,060	0,550	0,0	0,0
4	70,7I2	I,624	0,842	0,0	0,0
6	86,283	2,952	I,532	0,002	0,00I
8	99,26I	4,498	2,334	0,004	0,003
I0	II0,565	6,222	3,229	0,007	0,005
I2	I20,669	8,095	4,20I	0,0II	0,008
I4	I29,883	I0,097	5,240	0,0I7	0,0I2
I6	I38,304	I2,2I2	6,337	0,023	0,0I6
20	I53,484	I6,725	8,679	0,040	0,028
24	I66,888	2I,548	II,I82	0,062	0,044
28	I78,926	26,6I9	I3,8I3	0,090	0,064
32	I89,865	3I,886	I6,546	0,I25	0,088
36	I99,893	37,309	I9,360	0,I65	0,II7
40	209,I48	42,856	22,238	0,2I2	0,I5I
45	2I9,787	49,9I9	25,903	0,28I	0,I99
50	229,538	57,086	29,62I	0,360	0,255
60	246,830	7I,586	37,I44	0,55I	0,390
70	26I,7I7	86,I25	44,586	0,785	0,557
80	274,658	I00,538	52,I62	I,063	0,754
90	285,983	II4,706	59,5I2	I,384	0,98I
I00	295,934	I28,543	66,689	I,746	I,238
II0	304,702	I4I,988	73,66I	2,I49	I,523
I20	3I2,434	I54,996	80,406	2,589	I,836
I30	3I9,252	I67,535	86,909	3,067	2,I74
I40	325,257	I79,586	93,I57	3,578	2,536
I50	330,534	I9I,I37	99,I45	4,I22	2,92I

Table 2.7. Evaluated average inelastic widths of ^{238}Pu.

E, keV	$\langle\Gamma_{n'}^0\rangle_{1/2^+}$, meV	$\langle\Gamma_{n'}^1\rangle_{1/2^-}$, meV	$\langle\Gamma_{n'}^1\rangle_{3/2^-}$, meV	$\langle\Gamma_{n'}^2\rangle_{3/2^+}$, meV	$\langle\Gamma_{n'}^2\rangle_{5/2^+}$, meV
I	2	3	4	5	6
45	0,0	0,I65	0,I7I	I6,347	II,593
50	0,007	2,6I7	2,7I5	4I,086	29,I37
60	0,08I	I0,962	II.376	66.I74	46,926
70	0,266	2I,659	22,475	82,970	58,834
80	0,585	33,636	34,903	96,023	68,085
90	I,049	46,326	48,070	I06,784	75,7II
I00	I,665	59,372	6I,604	II5,952	82,207
II0	2,436	72,530	75,255	I23,920	87,858
I20	3,364	85,63I	88,845	I30,977	92,848
I30	4,445	98,552	I02,248	I37,270	97,303
I40	5,677	III,205	II5,37I	I42,939	I0I,3I6
I50	7,054	I23,524	I28,I47	I48,083	I04,956

Table 2.8. Average fission widths and value of factor x_{max}.

E, keV	$\Gamma_{f\,1/2}$, meV	$\Gamma_{f\,3/2}$, meV	$\Gamma_{f\,5/2}$, meV	x_{max}
1	2	3	4	5
0,5	46,156	47,908	50,979	9,007
1	46,260	48,016	51,090	8,970
1,5	46,362	48,123	51,206	8,932
2	46,466	48,230	51 319	8,895
2,5	46,569	48,337	51,433	8,858
3	46,673	48,444	51,547	8,821
4	46,881	48,660	51,776	8,748
6	47,299	49,094	52,238	8,604
8	47,721	49,532	52,703	8,463
10	48,147	49,973	53,171	8,325
12	48,576	50,418	53,644	8,190
14	49,008	50,866	54,121	8,057
16	49,445	51,319	54,602	7,927
20	50,329	52,236	55,576	7,675
24	51,227	53,168	56,566	7,432
28	52,141	54,115	57,573	7,199
32	53,070	55,079	58,597	6,976
36	54,015	56,059	59,638	6,763
40	54,976	57,055	60,697	6,554
45	56,200	58,324	62,045	6,308
50	57,449	59,620	63,421	6,073
60	60,026	62,292	66,260	5,637
70	62,711	65,076	69,218	5,243
80	65,509	67,977	72,299	4,885
90	68,423	70,998	75,508	4,561
100	71,457	74,144	78,848	4,267
110	74,615	77,418	82,326	4,000
120	77,902	80,826	85,944	3,758
130	81,321	84,370	89,708	3,538
140	84,877	88,057	93,623	3,337
150	88,575	91,890	97,693	3,154

Table 3.1. Evaluated $\sigma_{nf}(^{238}Pu)/\sigma_{nf}(^{235}U)$ ratios and their errors.

E_n, MeV	$\frac{\sigma_{nf}(^{238}Pu)}{\sigma_{nf}(^{235}U)}$	$\Delta \frac{\sigma_{nf}(^{238}Pu)}{\sigma_{nf}(^{235}U)}$, %	E_n, MeV	$\frac{\sigma_{nf}(^{238}Pu)}{\sigma_{nf}(^{235}U)}$	$\Delta \frac{\sigma_{nf}(^{238}Pu)}{\sigma_{nf}(^{235}U)}$, %
I	2	3	4	5	6
0.I5	0,388	I0	2.4	I,754	4
0,I6	0,396	I0	2,6	I,780	4
0,I8	0,4I9	9	2,8	I,806	4
0,20	0,458	9	3,0	I,837	4
0,22	0,49I	8	3,2	I,857	4
0,24	0,529	8	3,4	I,878	4
0,26	0,569	8	3,6	I,904	4
0,28	0,609	8	3,8	I,92I	5
0,30	0,650	8	4,0	I,936	5
0,32	0,69I	7	4,5	I,937	5
0,34	0,734	7	5,0	I,984	5
0,36	0,777	7	5,5	2,009	6
0,38	0,825	7	6,0	2,096	6
0,40	0,873	6	6,5	I,870	6
0,42	0,9I8	6	7,0	I,707	6
0,44	0,976	6	7,5	I,577	6
0,46	I,034	6	8,0	I,543	6
0,48	I,083	5	8,5	I,549	6
0,50	I,I35	5	9,0	I,556	6
0,55	I,264	5	9,5	I,563	6
0,60	I,389	5	I0,0	I,570	6
0,65	I,474	5	I0,5	I,575	6
0,70	I,539	5	II,0	I,576	6
0,75	I,60I	5	II,5	I,569	6
0,80	I,65I	5	I2,0	I,546	6
0,85	I,683	5	I2,5	I,473	6
0,90	I,69I	5	I3,0	I,397	6
0,95	I,669	5	I3,5	I,333	6
I,00	I,664	5	I4,0	I,282	5
I,I	I,704	5	I4,5	I,258	5
I,2	I,7I9	5	I5,0	I,248	4
I,4	I,733	5	I6,0	I,256	4
I,6	I,737	4	I7,0	I,295	4
I,8	I,728	4	I8,0	I,307	5
2,0	I,725	4	I9,0	I,269	6
2,2	I,734	4	20,0	I,I95	6

Table 4.1. Evaluated neutron cross-section data for ^{238}Pu in the fast neutron energy region.

E, MeV	σ_t, 10^{-28} m^2	σ_{nn}, 10^{-28} m^2	σ_{nf}, 10^{-28} m^2	σ_{nf}, 10^{-28} m^2	$\sigma_{nn'}$, 10^{-28} m^2		σ_{n2n}, 10^{-28} m^2	σ_{n3n}, 10^{-28} m^2
					Direct	Total		
1	2	3	4	5	6	7	8	9
0,15	11,946	10,540	0,565	0,281	0,018	0,560		
0,16	11,317	9,905	0,570	0,265	0,021	0,577		
0,18	11,064	9,617	0,590	0,247	0,025	0,610		
0,20	10,784	9,231	0,630	0,237	0,032	0,686		
0,22	10,548	8,931	0,660	0,230	0,038	0,727		
0,24	10,340	8,668	0,695	0,224	0,044	0,753		
0,26	10,132	8,404	0,735	0,219	0,049	0,774		
0,28	9,936	8,156	0,775	0,214	0,056	0,791		
0,30	9,608	7,771	0,820	0,211	0,077	0,806		
0,32	9,440	7,553	0,865	0,207	0,083	0,815		
0,34	9,280	7,343	0,910	0,204	0,089	0,823		
0,36	9,132	7,144	0,955	0,201	0,098	0,832		
0,38	9,000	6,960	1,005	0,198	0,105	0,837		
0,40	8,852	6,762	1,055	0,195	0,112	0,840		
0,42	8,760	6,615	1,100	0,193	0,119	0,852		
0,44	8,670	6,456	1,160	0,190	0,126	0,864		
0,46	8,586	6,306	1,220	0,188	0,133	0,872		
0,48	8,470	6,141	1,270	0,186	0,141	0,873		
0,50	8,372	5,992	1,325	0,184	0,148	0,871		
0,55	8,140	5,635	1,460	0,179	0,165	0,866		
0,60	7,926	5,308	1,590	0,175	0,183	0,853		
0,65	7,740	4,988	1,680	0,171	0,200	0,901		
0,70	7,605	4,757	1,750	0,167	0,219	0,931		
0,75	7,460	4,524	1,820	0,164	0,237	0,952		
0,80	7,353	4,344	1,880	0,163	0,253	0,966		
0,85	7,250	4,169	1,930	0,162	0,269	0,989		
0,90	7,175	4,051	1,975	0,162	0,286	0,987		
0,95	7,100	3,929	2,005	0,161	0,302	1,005		
1,00	7,053	3,785	2,030	0,158	0,315	1,080		
1,10	6,991	3,567	2,070	0,148	0,343	1,206		
1,2	6,972	3,478	2,097	0,136	0,370	1,261		
1,4	7,044	3,415	2,147	0,113	0,416	1,369		
1,6	7,184	3,457	2,195	0,093	0,453	1,439		
1,8	7,349	3,564	2,225	0,076	0,480	1,484		
2,0	7,509	3,703	2,239	0,063	0,498	1,504		
2,2	7,650	3,855	2,240	0,053	0,508	1,502		
2,4	7,757	4,002	2,242	0,043	0,511	1,470		
2,6	7,840	4,148	2,241	0,036	0,509	1,415		
2,8	7,889	4,250	2,240	0,030	0,504	1,369		
3,0	7,918	4,340	2,239	0,025	0,496	1,314		
3,2	7,940	4,409	2,230	0,021	0,490	1,280		
3,4	7,945	4,450	2,223	0,017	0,482	1,255		
3,6	7,930	4,471	2,218	0,014	0,472	1,227		
3,8	7,893	4,473	2,205	0,011	0,463	1,204		
4,0	7,854	4,457	2,192	0,009	0,454	1,196		
4,5	7,710	4,354	2,152	0,007	0,434	1,197		
5,0	7,517	4,191	2,111	0,006	0,411	1,209		
5,5	7,300	3,986	2,103	0,006	0,394	1,205		
6,0	7,080	3,773	2,330	0,005	0,379	0,972		
6,5	6,870	3,570	2,550	0,005	0,364	0,745		
7,0	6,653	3,358	2,651	0,004	0,351	0,641		
7,5	6,467	3,174	2,711	0,004	0,338	0,576	0,002	

Table 4.1. (cont.)

I	2	3	4	5	6	7	8	9
8,0	6,3I2	3,0I9	2,750	0,003	0,326	0,535	0,005	
8,5	6,I60	2,878	2,760	0,003	0,3I5	0,498	0,02I	
9,0	6,049	2,779	2,758	0,002	0,303	0,467	0,043	
9,5	5,958	2,700	2,754	0,002	0,290	0,438	0,064	
I0,0	5,89I	2,640	2,746	0,00I	0,282	0,422	0,082	
I0,5	5,83I	2,585	2,738	0,00I	0,283	0,4I0	0,097	
II,0	5,8I3	2,574	2,729	0,00I	0,284	0,400	0,I09	
II,5	5,8I7	2,587	2,7I7	0,00I	0,285	0,392	0,I20	
I2,0	5,8I9	2,604	2,703	0,00I	0,284	0,38I	0,I30	
I2,5	5,832	2,630	2,690	0,00I	0,282	0,374	0,I37	
I3,0	5,860	2,678	2,676	0,00I	0,279	0,365	0,I40	
I3,5	5,893	2,732	2,664	0,00I	0,276	0,358	0,I38	
I4,0	5,929	2,794	2,65I	0,00I	0,272	0,349	0,I34	
I4,5	5,978	2,862	2,64I	0,00I	0,268	0,343	0,I29	0,002
I5,0	6,0I2	2,928	2,625	0,00I	0,263	0,332	0,I22	0,004
I6,0	6,083	3,063	2,598	0,00I	0,25I	0,3I6	0,097	0,008
I7,0	6,I48	3,I89	2,572	0,00I	0,242	0,298	0,076	0,0I2
I8,0	6,I9I	3,299	2,534	0,00I	0,234	0,278	0,063	0,0I6
I9,0	6,I98	3,37I	2,494	0,00I	0,225	0,262	0,052	0,0I8
20,0	6,206	3,450	2,444	0,00I	0,2I5	0,248	0,043	0,020

Table 4.2. Evaluated level excitation cross-sections for ^{238}Pu, 10^{-28} m^2.

E_n, MeV	Level energy E_q, keV							
	44,08	I45,96	44,08	I45,96	303,6	605,I8	66I,43	94I,5
	Direct excitation		Compound nucleus mechanism					
0,I6	0,02I		0,5560					
0,I8	0,025		0,5848	0,0002				
0,20	0,032		0,6535	0,0005				
0,22	0,038		0,6879	0,00II				
0,24	0,043	0,00I	0,7072	0,00I8				
0,26	0,048	0,00I	0,7223	0,0027				
0,28	0,054	0,002	0,73I2	0,0038				
0,30	0,075	0,002	0,7I53	0,0I37				
0,32	0,08I	0,002	0,7I49	0,0I7I				
0,34	0,087	0,002	0,7I33	0,0207				
0,36	0,094	0,004	0,7093	0,0247				
0,38	0,I00	0,005	0,7032	0,0288				
0,40	0,I06	0,006	0,6948	0,0332				
0,42	0,III	0,008	0,6948	0,0382				
0,44	0,II7	0,009	0,6943	0,0437				
0,46	0,I22	0,0II	0,6900	0,0490				
0,48	0,I28	0,0I3	0,6778	0,0542				
0,50	0,I33	0,0I5	0,6637	0,0592	0,000I			
0,55	0,I45	0,020	0,6290	0,07I8	0,0002			
0,60	0,I57	0,026	0,5864	0,0832	0,0004			
0,65	0,I67	0,033	0,5450	0,0947	0,0008	0,0605		
0,70	0,I78	0,04I	0,5030	0,I035	0,00I3	0,0924	0,0II8	
0,75	0,I88	0,049	0,4660	0,III8	0,0020	0,II03	0,0249	
0,80	0,I97	0,056	0,4348	0,II98	0,0029	0,II99	0,0356	
0,85	0,206	0,063	0,4I5I	0,I294	0,0040	0,I264	0,045I	
0,90	0,2I5	0,07I	0,3843	0,I34I	0,0053	0,I262	0,05II	
0,95	0,223	0,079	0,3695	0,I420	0,0069	0,I256	0,0572	0,00I8

Table 4.2. (cont.)

E_n, MeV	Level energy E_q, keV							
	44,08	I45,96	44,08	I45,96	303,6	605,I8	66I,43	94I,5
	Direct excitation		Compound nucleus mechanism					
I,0	0,230	0,085	0,3600	0,I527	0,0090	0,I255	0,0634	0,0I26
I,I	0,246	0,097	0,3292	0,I534	0,0II6	0,II37	0,0624	0,0282
I,2	0,26I	0,I09	0,2704	0,I44I	0,0I46	0,0943	0,0592	0,0333
I,4	0,288	0,I28	0,2086	0,I320	0,0206	0,0728	0,0566	0,033I
I,6	0,3I2	0,I4I	0,I663	0,II54	0,0239	0,0583	0,0509	0,0287
I,8	0,330	0,I50	0,I290	0,0942	0,0233	0,0462	0,0447	0,0239
2,0	0,343	0,I56	0,095I	0,07I4	0,0I97	0,0352	0,0367	0,0I9I
2,2	0,350	0,I58	0,0654	0,0500	0,0I49	0,0253	0,0278	0,0I43
2,4	0,352	0,I59	0,0426	0,033I	0,0I04	0,0I72	0,0I98	0,0I00
2,6	0,35I	0,I58	0,0264	0,0209	0,0068	0,0III	0,0I32	0,0065
2,8	0,348	0,I56	0,0I62	0,0I30	0,0044	0,007I	0,0087	0,004I
3,0	0,342	0,I54	0,0097	0,0079	0,0028	0,0044	0,0055	0,0025
3,2	0,337	0,I53	0,0057	0,0048	0,00I9	0,0026	0,0034	0,00I5
3,4	0,33I	0,I5I	0,0034	0,0030	0,00I2	0,00I6	0,002I	0,0009
3,6	0,324	0,I48	0,0020	0,00I8	0,0008	0,00I0	0,00I4	0,0005
3,8	0,3I7	0,I46	0,00I3	0,00I2	0,0005	0,0006	0,0009	0,0003
4,0	0,3II	0,I43	0,0006	0,0006	0,0003	0,0003	0,0005	0,0002

Table 4.2. (cont.)

E_n, MeV	Level energy E_q, keV						Continuous spectrum excitation
	962,77	968,1	983,I	985,46	I028,55	I069,95	
I,0	0,0I82	0,0I2I	0,005I	0,0064			
I,I	0,0382	0,0304	0,04I6	0,0265	0,0223	0,0046	0,0009
I,2	0,0448	0,0387	0,0640	0,0359	0,0493	0,0257	0,0I66
I,4	0,0466	0,0446	0,0786	0,0430	0,07I3	0,0509	0,0953
I,6	0,0422	0,0433	0,0750	0,0423	0,0708	0,0560	0,2I29
I,8	0,0357	0,0387	0,0658	0,0380	0,0629	0,0526	0,3490
2,0	0,0284	0,032I	0,0545	0,03I6	0,0523	0,0457	0,4842
2,2	0,02II	0,0247	0,04I9	0,0244	0,0404	0,0367	0,607I
2,4	0,0I48	0,0I78	0,0302	0,0I76	0,0293	0,0275	0,6887
2,6	0,0098	0,0I2I	0,0202	0,0I20	0,0I97	0,0I90	0,7283
2,8	0,0064	0,0080	0,0I3I	0,0079	0,0I29	0,0I26	0,7506
3,0	0,0040	0,005I	0,0082	0,005I	0,0080	0,0080	0,7468
3,2	0,0024	0,003I	0,0049	0,003I	0,0049	0,0049	0,7468
3,4	0,00I5	0,0020	0,0030	0,0020	0,0030	0,0030	0,7463
3,6	0,0009	0,00I3	0,00I8	0,00I2	0,00I8	0,00I9	0,7386
3,8	0,0006	0,0008	0,00II	0,0008	0,00II	0,00I2	0,7306
4,0	0,0004	0,0004	0,0006	0,0004	0,0006	0,0007	0,7364

Table 4.2. (cont.)

E_n, MeV	Level energy E_q, keV		Continuous spectrum excitation
	44,08	I45,96	
	Direct excitation		
4,5	0,297	0,I37	0,763
5,0	0,282	0,I29	0,798
5,5	0,27I	0,I23	0,8II
6,0	0,263	0,II6	0,593
6,5	0,255	0,I09	0,38I
7,0	0,249	0,I02	0,290
7,5	0,243	0,095	0,238
8,0	0,237	0,089	0,209
8,5	0,232	0,083	0,I83
9,0	0,224	0,079	0,I64
9,5	0,2I6	0,074	0,I48
I0,0	0,2I3	0,069	0,I40
I0,5	0,2I5	0,068	0,I27
II,0	0,2I7	0,067	0,II6
II,5	0,2I9	0,066	0,I07
I2,0	0,2I9	0,065	0,097
I2,5	0,2I8	0,064	0,092
I3,0	0,2I6	0,063	0,086
I3,5	0,2I5	0,06I	0,082
I4,0	0,2I3	0,059	0,077
I4,5	0,2I0	0,058	0,075
I5	0,207	0,056	0,069
I6	0,I99	0,052	0,065
I7	0,I92	0,050	0,056
I8	0,I87	0,047	0,044
I9	0,I8I	0,044	0,037
20	0,I75	0,040	0,033

Table 5.1. Temperature T_M of the fission neutron spectrum.

E_n, MeV	T_M, MeV	E_n, MeV	T_M, MeV
10^{-5}	I,350	9	I,4I4
0,5	I,354	I5	I,455
5	I,39I	20	I,478
6	I,397		

Table 5.2. Average number of neutrons emitted per fission event.

E_n, MeV	$\bar{\nu}_p$	$\bar{\nu}_t$
10^{-5}	2,840	2,885
0,5	2,9I0	2,955
5	3,535	3,580
6	3,674	3,7I4
9	4,II8	4,I45
I5	5,006	5,033
20	5,54I	5,568

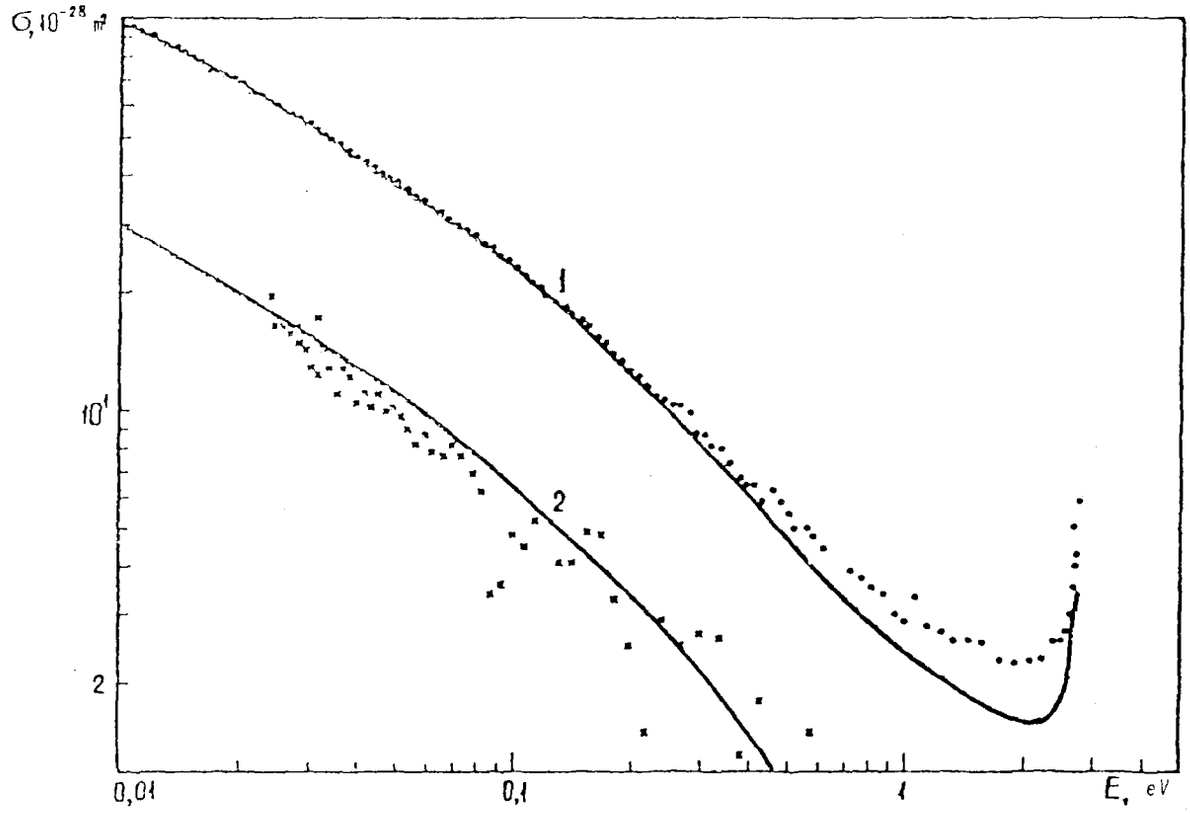

Figure 1.1. Comparison of evaluated and experimental data on σ_t (I) and σ_{nf} (2) in the region up to the first resonance:

× - /7/; • -/6/.

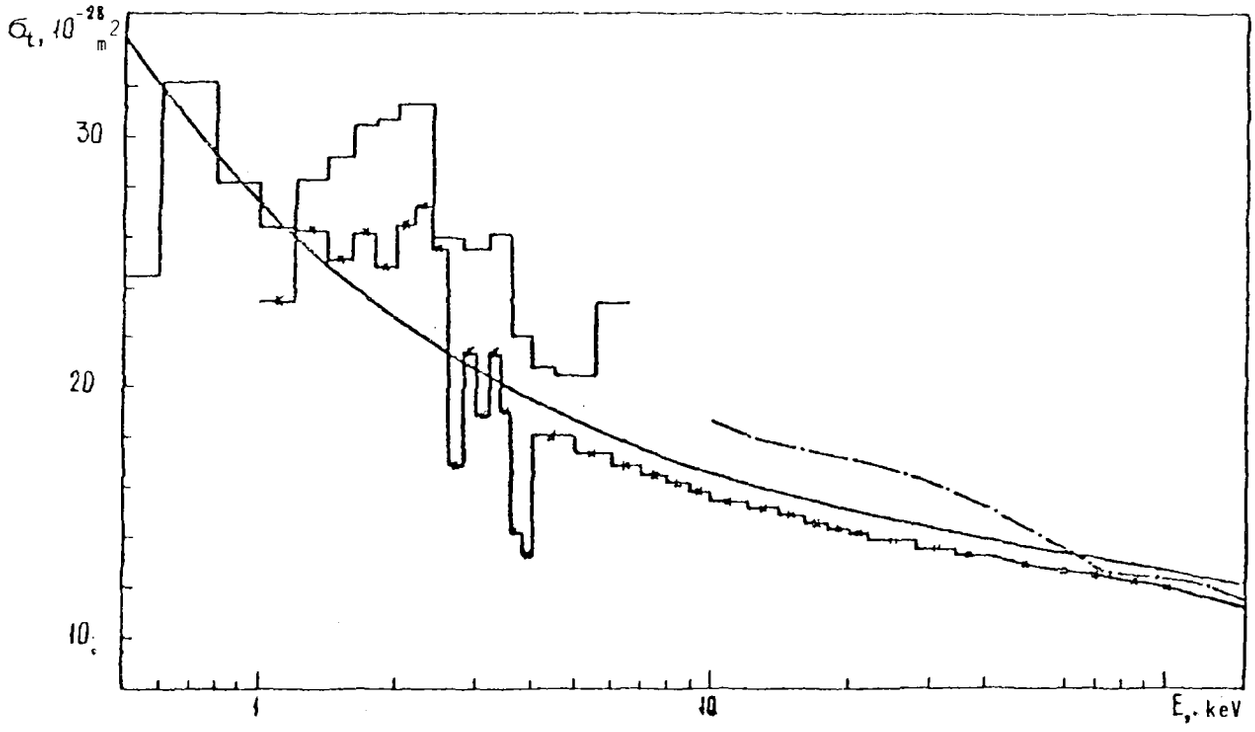

Figure 2.1. Comparison of evaluated and experimental data on σ_t in the unresolved resonance energy region:

⌐¬ - /6/; ⌐¬ - eval. /I7/; —·—·— eval. ENDF/B-V /I8/; —— - present work.

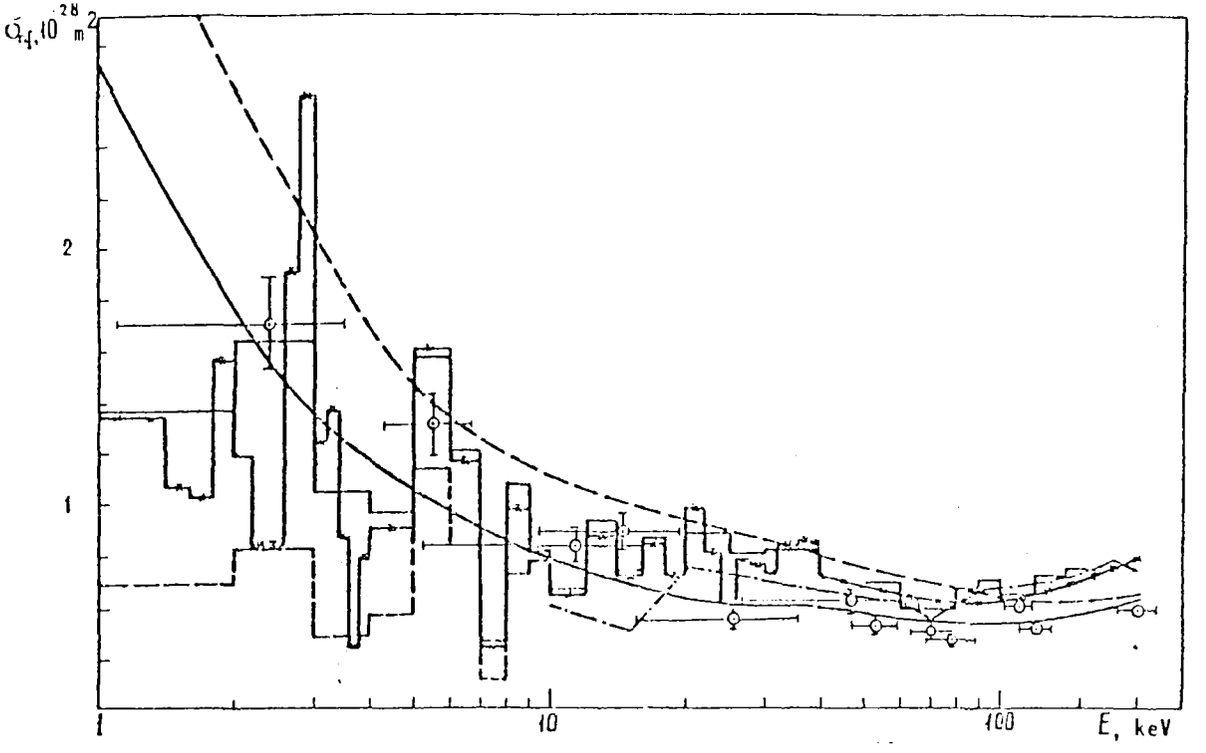

Figure 2.2. Comparison of the different evaluations of σ_{nf} in the unresolved resonance region with experimental data:

— – : present evaluation;

– – – calculation with same parameters without considering additional fission width distribution;

–·–· eval. ENDF/B V /I3/; ⌐ ~ eval. /I7/; ∮ - /I6/; ⌐ - /9/; ⌐ - /20/.

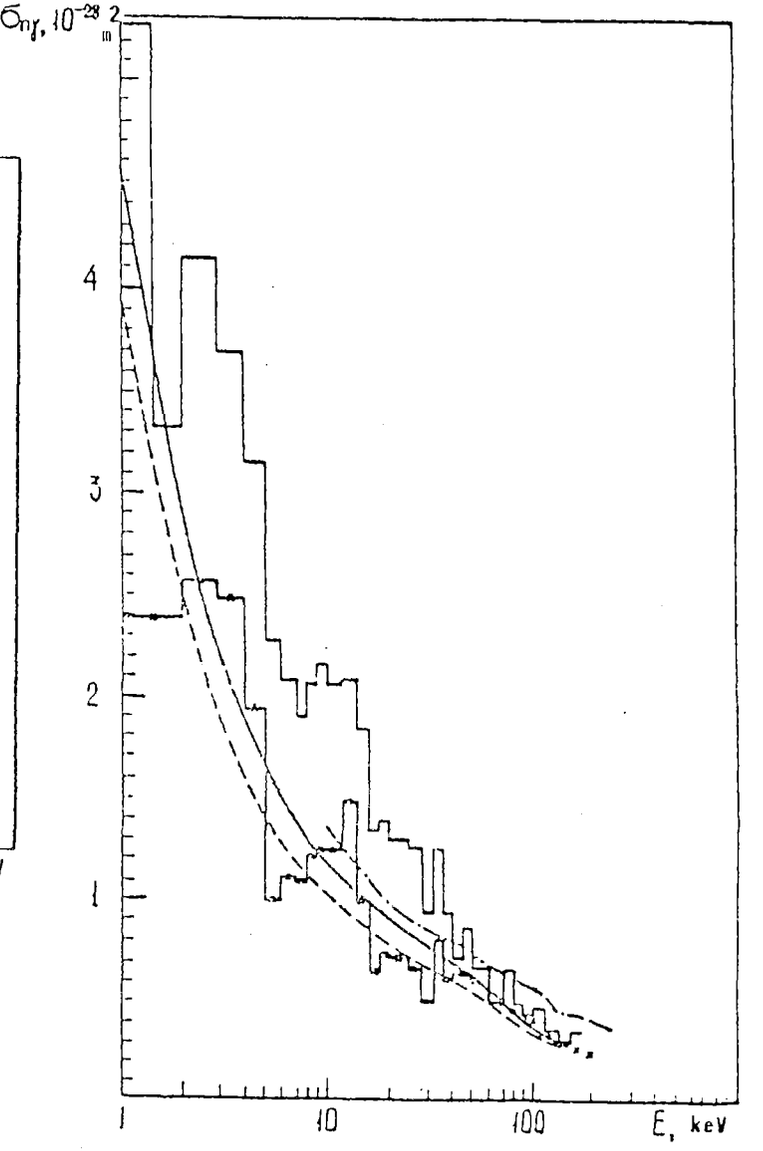

Figure 2.3. Comparison of evaluated and experimental data on $\sigma_{n\Gamma}$ ⌐ - /I0/ (for notations of evaluated curves see Fig. 2.2)

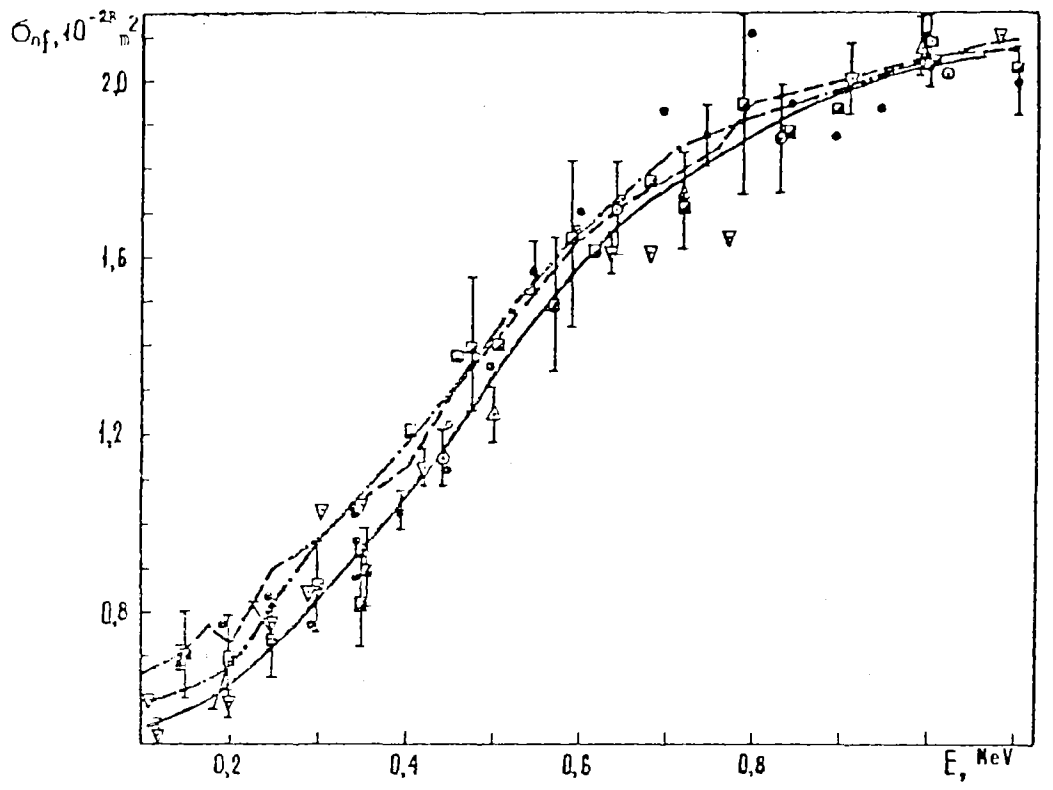

Figure 3.1. Comparison of evaluated data on σ_{nf} with experimental data in the 0.1-1.1 MeV region: □ - /26/; • - /II/; ▽ - /I6/; △ -/24/; ◘ - /29/; ○ - /25/; —— present evaluation; ---- eval. ENDF/B-V /I8/; -·-·- eval. /I7/.

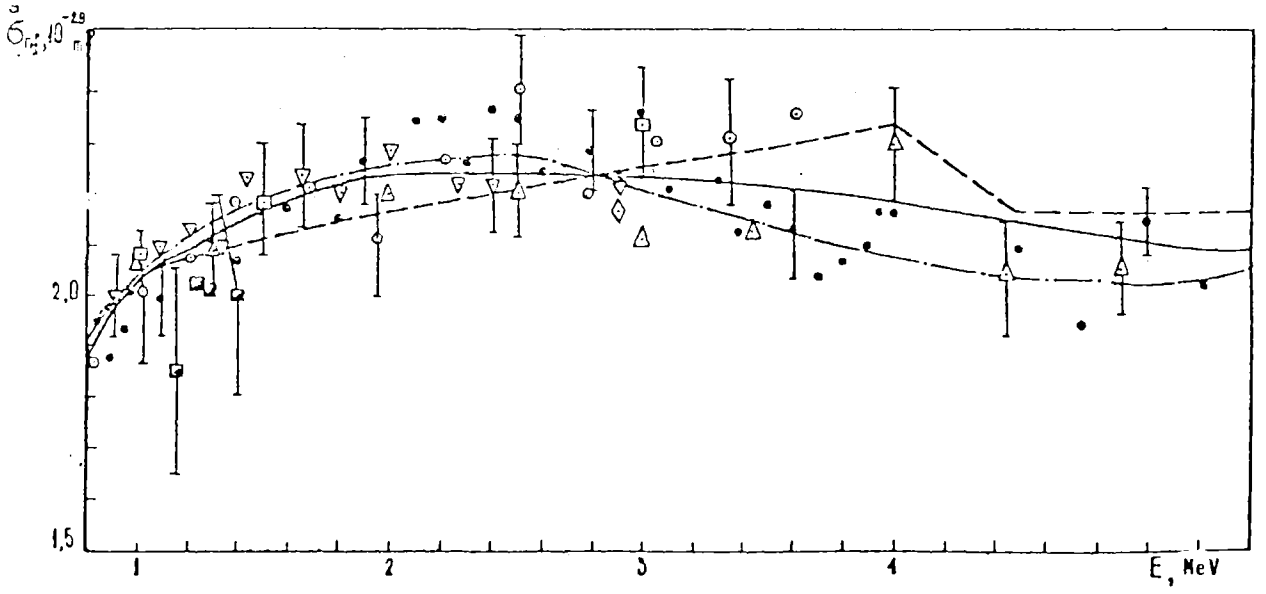

Figure 3.2. Comparison of evaluated and experimental data on σ_{nf} in the 0.8-5.6 MeV region: ◆ - /27/ (for other notations see Fig. 3.1).

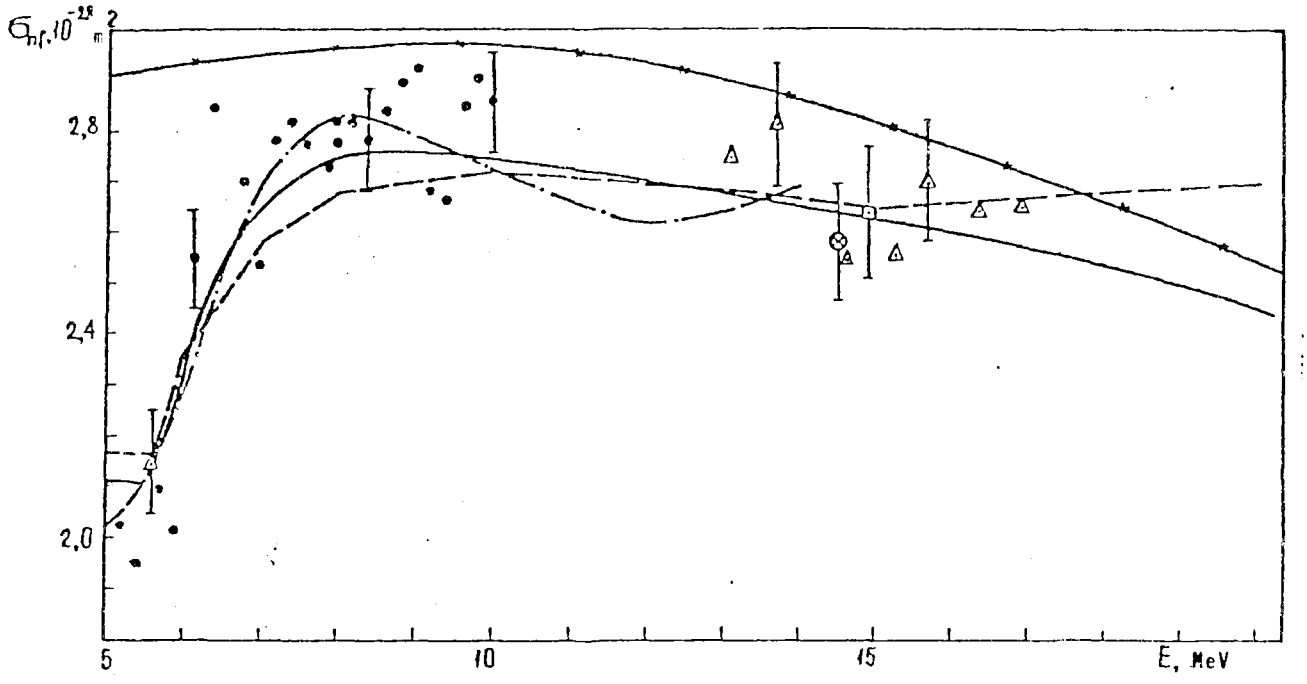

Figure 3.3. Comparison of experimental and evaluated data on σ_{nf} in the 5-20 MeV region:
⊗ – /28/; –×–×– Calculated compound nucleus formation cross-section (for other notations see Fig. 3.1).

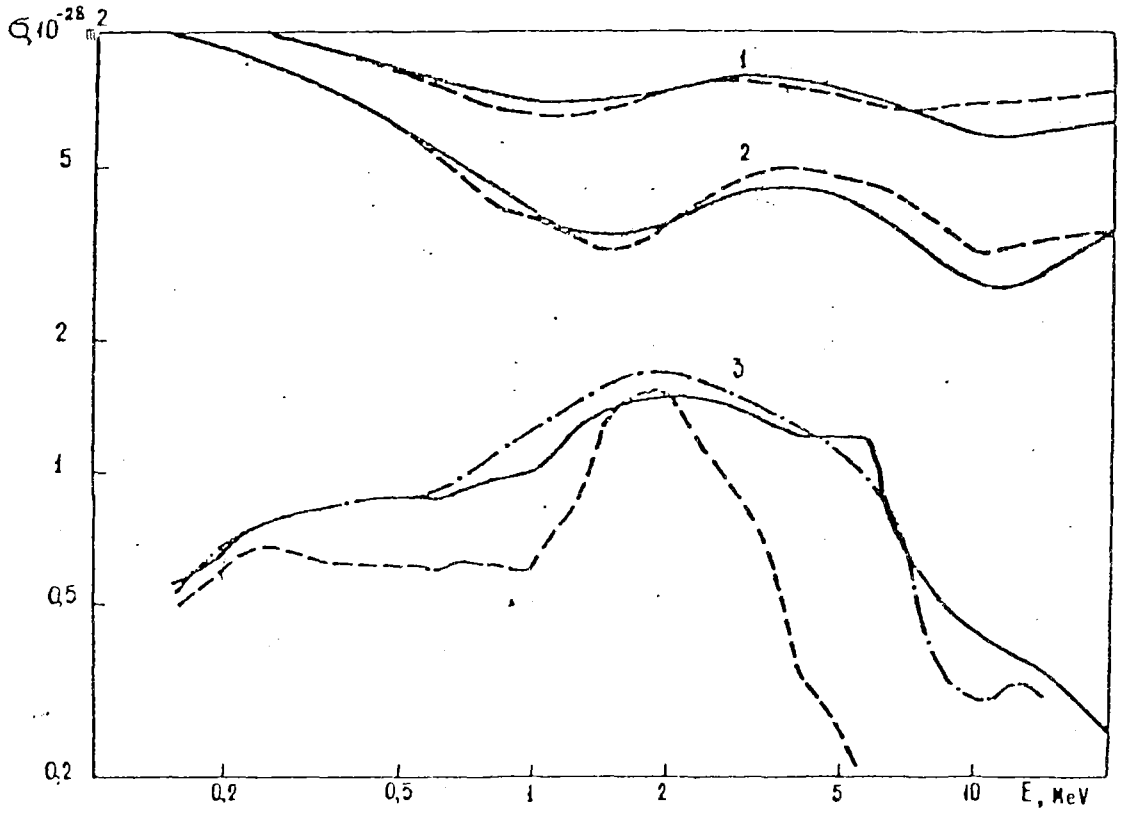

Figure 4.1.
Comparison of the different evaluations for σ_t(1), σ_{in}(2) and $\sigma_{in'}$(3) in the 0.15-20 MeV region:
—— - present evaluation; – – – – eval. ENDF/B $\bar{V}$/I8/; —·—·— eval. /I7/.

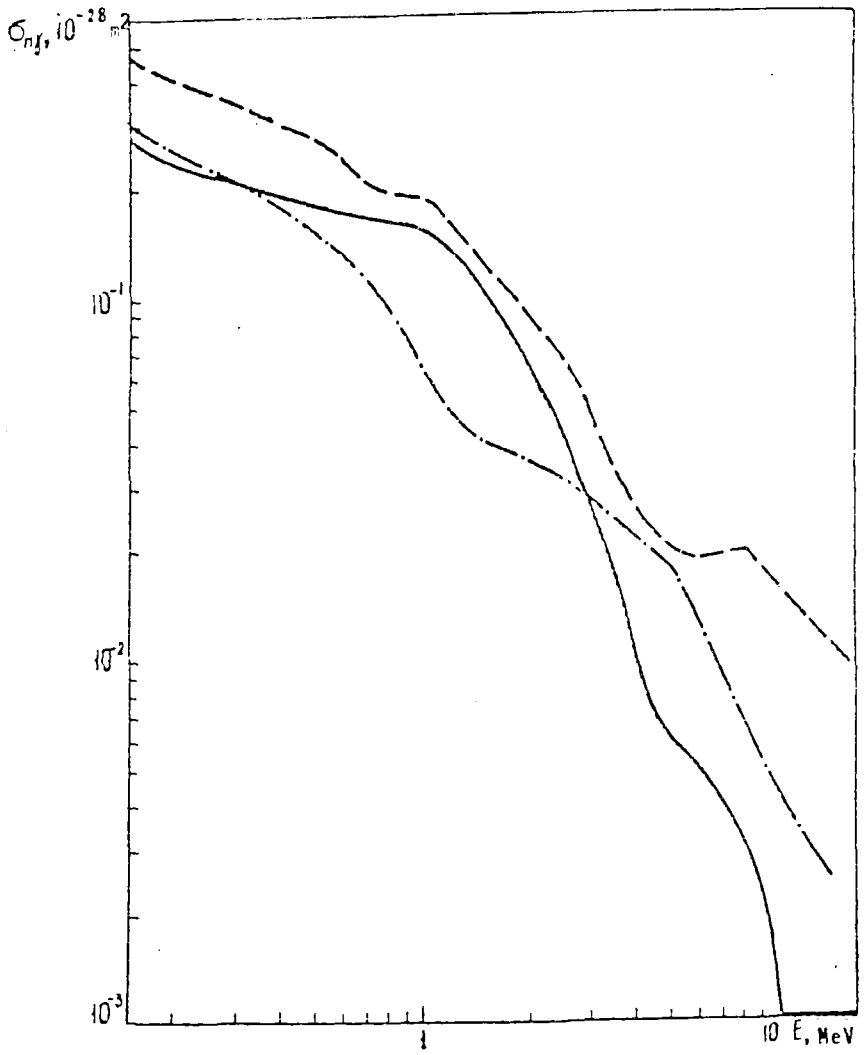

Figure 4.2.
Comparison of the different evaluations for $\sigma_{n\gamma}$ in the 0.15-20 MeV region (for notations of curves see Fig. 4.1).

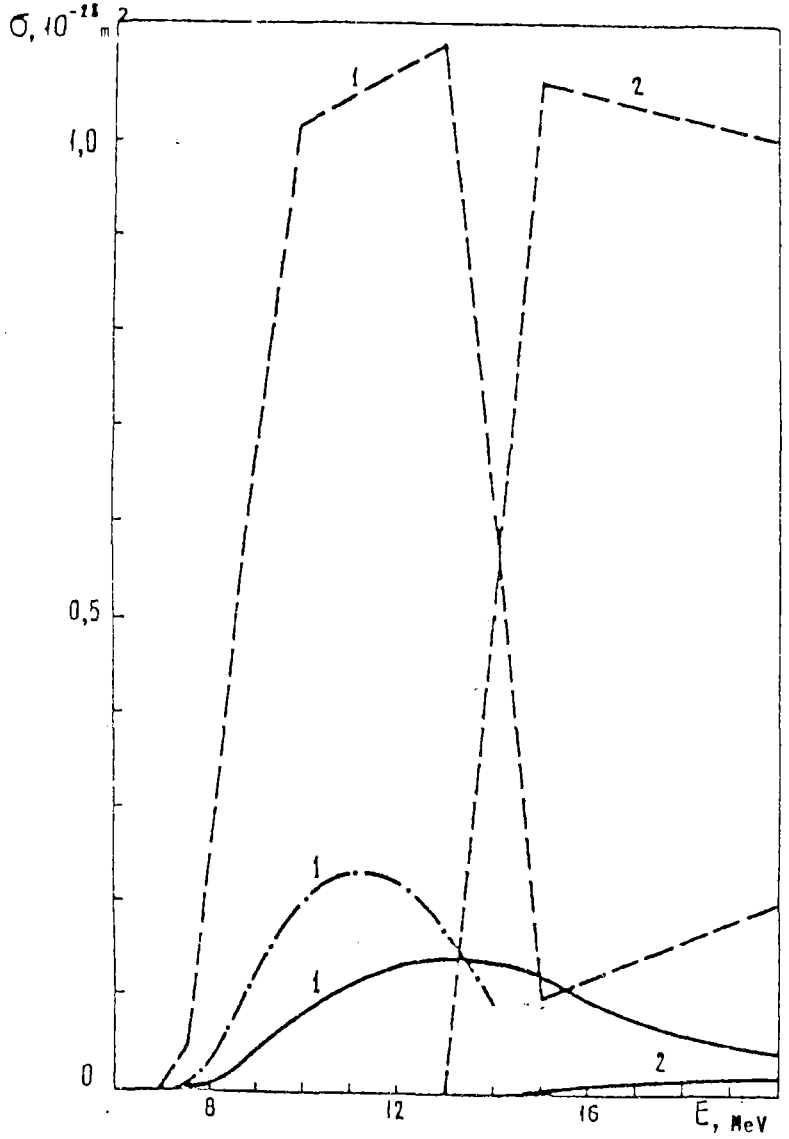

Figure 4.3. Comparison of the different evaluations for $\sigma_{n,2n}$(1) and $\sigma_{n,3n}$(2) (for notations see Fig. 4.1).

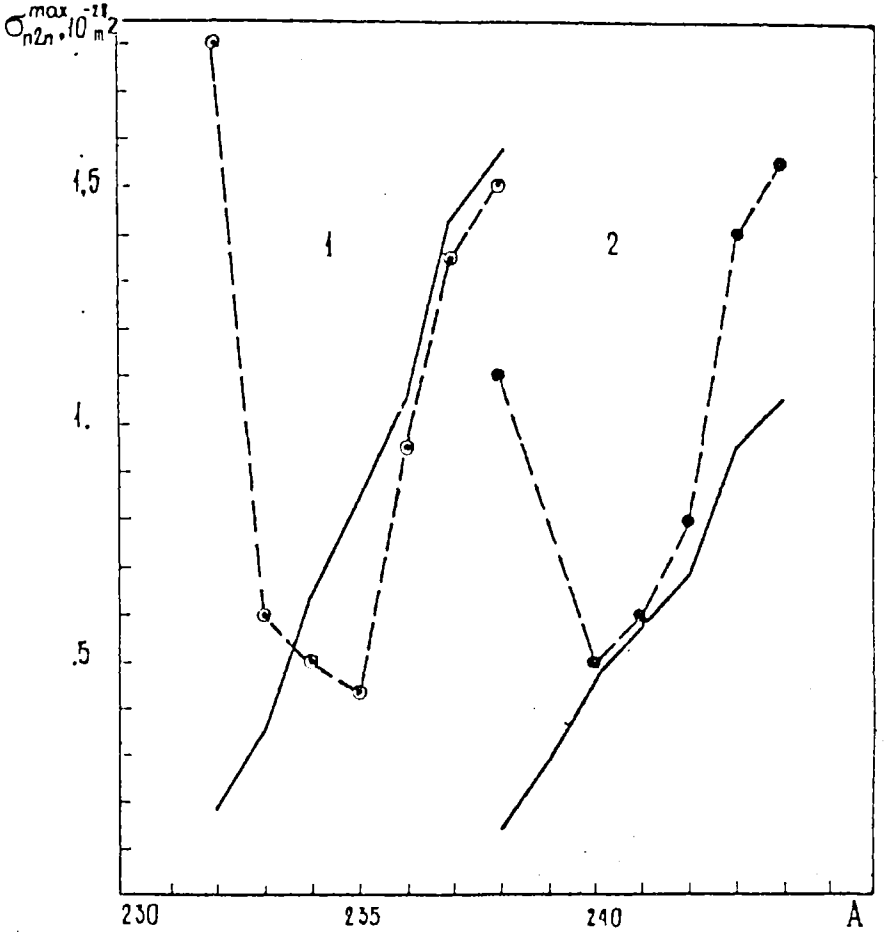

Figure 4.4. Dependence of σ^{max}_{n2n} of uranium (1) and plutonium (2) isotopes: ---- eval. ENDF/B ; —— - present evaluation.

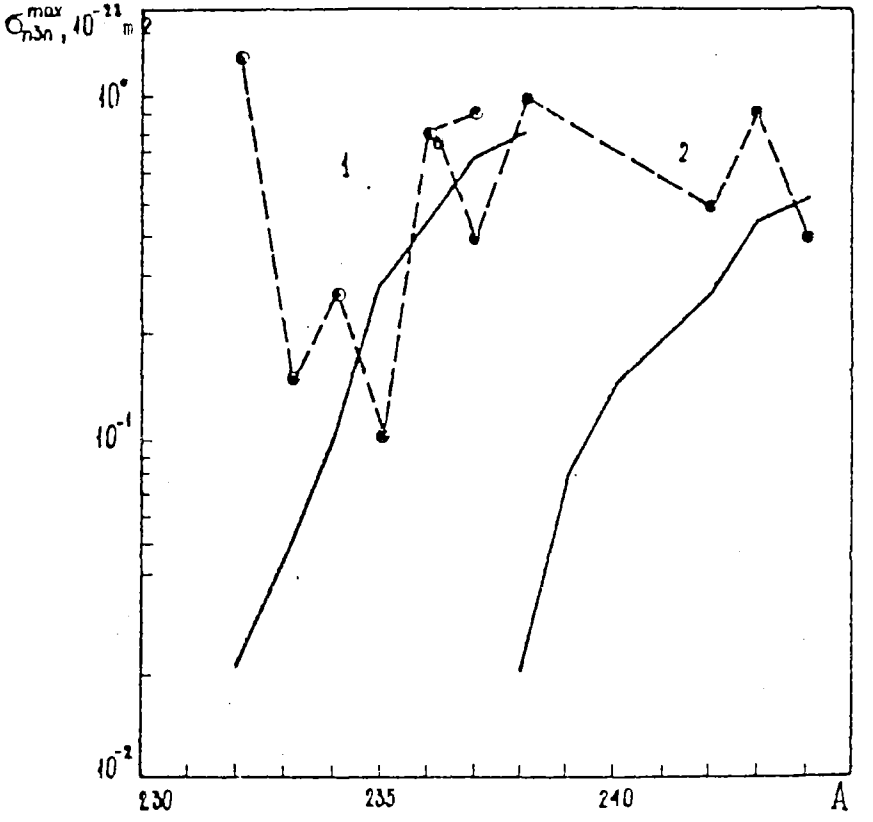

Figure 4.5. Dependence of $\sigma^{max}_{n,3n}$ in the different evaluations (for notations see Fig. 4.4).